6170-0082-2022
14 March 2022

Classification of Underwater UXO from Dynamic EMI Survey Data, Interim Report on EMI Array Design

ESTCP Project MR21-5066

Dr. Daniel Steinhurst[1]
Mr. Glenn Harbaugh[1]
Dr. Thomas Bell[1]
Dr. Stephen Billings[2]
Dr. Shawn P. Mulvaney[3]

[1] Nova Research, Inc.
Alexandria, VA 22308

[2] Black Tusk / GAP EOD
Vancouver, BC, V6J 4S5
Canada

[3] Chemistry Division
Washington, DC 20375

REPORT DOCUMENTATION PAGE

Form Approved
OMB No. 0704-0188

PLEASE DO NOT RETURN YOUR FORM TO THE ABOVE ORGANIZATION.

1. REPORT DATE *(DD-MM-YYYY)*	2. REPORT TYPE	3. DATES COVERED *(From - To)*
14-03-2022	ESTCP Interim Report	03/01/2021 - 02/28/2022

4. TITLE AND SUBTITLE

Classification of Underwater UXO from Dynamic EMI Survey Data
Interim Report on EMI Array Design
ESTCP Project MR-21-5066

5a. CONTRACT NUMBER

5b. GRANT NUMBER

5c. PROGRAM ELEMENT NUMBER
0603851D8Z0

6. AUTHOR(S)
D.A. Steinhurst[1], G.R. Harbaugh[1], T.H. Bell[1], S.F. Billings[2],S.P. Mulvaney[3]

5d. PROJECT NUMBER
MR-21-5066

5e. TASK NUMBER

5f. WORK UNIT NUMBER
1U03

7. PERFORMING ORGANIZATION NAME(S) AND ADDRESS(ES)
[1]Nova Research, Inc., 1900 Elkin Street, Suite 230, Alexandria, VA 22308;
[2]401 / 1755 West Broadway, Vancouver, BC, V6J 4S5, Canada;
[3]Chemistry Division, NRL, 4555 Overlook Ave., SW, Washington, DC, 20375

8. PERFORMING ORGANIZATION REPORT NUMBER
MR21-5066

9. SPONSORING/MONITORING AGENCY NAME(S) AND ADDRESS(ES)
Environmental Security Technology Certification Program (ESTCP) Program Office
4800 Mark Center Drive, Suite 16F16
Alexandria, VA 22350-3605

10. SPONSOR/MONITOR'S ACRONYM(S)
ESTCP

11. SPONSOR/MONITOR'S REPORT NUMBER(S)
MR21-5066

12. DISTRIBUTION/AVAILABILITY STATEMENT
Distribution A: Approved for public release; distribution unlimited.

13. SUPPLEMENTARY NOTES

14. ABSTRACT

Leveraging the lessons learned in ESTCP MR-201610 and with the extensive fielding of the BTG/GapEOD UltraTEM Marine family of systems in Europe, the objective of this project is to integrate a high power, AGC-grade electromagnetic induction (EMI) sensor array in the marine towed array (MTA) platform to provide dynamic UXO classification at standoff distances compatible with the MTA's maneuvering profile through the water. This report documents the results of our design and testing of the proposed EMI transmitter and transmitter loop designs and physical testing of test articles to confirm the proposed transmitter design will meet the requirements for successful classification performance.

15. SUBJECT TERMS
Marine Towed Array (MTA), Unexploded Ordnance (UXO), Electromagnetic Induction (EMI), EMI response, transient electromagnetic induction (TEM), Underwater, Classification

16. SECURITY CLASSIFICATION OF:			17. LIMITATION OF ABSTRACT	18. NUMBER OF PAGES	19a. NAME OF RESPONSIBLE PERSON
a. REPORT	b. ABSTRACT	c. THIS PAGE			Shawn P. Mulvaney, NRL, Code 6177
Unclassified	Unclassified	Unclassified	Unlimited	53	19b. TELEPHONE NUMBER *(Include area code)* (202) 404-2102

Abstract

Leveraging the lessons learned in ESTCP MR-201610 and with the extensive fielding of the BTG/GapEOD UltraTEM Marine family of systems in Europe, the objective of this project is to integrate a high power, AGC-grade electromagnetic induction (EMI) sensor array in the marine towed array (MTA) platform to provide dynamic UXO classification at standoff distances compatible with the MTA's maneuvering profile through the water. This report documents the results of our design and testing of the proposed EMI transmitter and transmitter loop designs and physical testing of test articles to confirm the proposed transmitter design will meet the requirements for successful classification performance.

The EMI array from MR-201610 was removed from the MTA and test stand measurements were made under controlled conditions to ensure that the performance observed during the field tests of MR-201610 could be reliably used to predict the performance metrics for the array to be designed and built in this project. Additionally, the precisely controlled target – array geometries of the test stand measurements will provide valuable benchmark data for comparison during the testing of the new array.

With these data in hand, a series of four potential transmitter coil designs were tested at GapEOD's facilities using available transmitters and power supplies. Initial measurements documented that it was possible to generate the proposed factor of eight increase in transmit moment with GapEOD's transmitters and transmitter loops of 8-16 turns using the 2m x 1m geometry of the inner transmitter loop layout used in MR-201610 and proposed in the project.

After discussion with the ESTCP Program Office, a more modest approach was explored, to determine what performance could be achieved without significant electronics redesign and the larger inherent technical risk. Based on the results of the testing documented in this report and the design analysis presented in Appendix A, we recommend proceeding with the fabrication of a prototype of the EODT120M transmitter, as outlined in Appendix A, for testing and the addition of a new Go / No Go decision point. Comparison of the designs and performance between this design and the existing UltraTEMA4 array indicate that the existing EODTx50M transmitter will not support the requirements of the proposed MTA system. Appendix A also outlines the specifications for the corresponding transmitter loops, which would be 7 turns of 8 AWG yielding 700 A·turns, and 9 turns of 10 AWG yielding 900 A·turns, for the large and small transmitter coils respectively. As discussed in Appendix A, the design modifications to convert a EODTx50M transmitter into the proposed EODTx120M transmitter are small, understood, and the technical risk manageable. Based on the detection modeling described in Appendix B, the proposed MTA design with the improved transmitter would provide a signal voltage/RMS noise voltage ratio of at least 11.5 at a 2.25 m standoff for a 105mm projectile.

Contents

Figures

Tables

Acronyms

AGC	Advanced Geophysical Classification
APG	Aberdeen Proving Ground
AWG	American Wire Gauge
BTField	AGC software package from BTG
BTG	Black Tusk Geophysics
CAD	Computer-Aided Design
cDAQ	Family of data acquition hardware from National Instruments
DAGCAP	DoD AGC Accreditation Program
DAQ	Data acquisition system / hardware
DoD	United States Department of Defense
EMI	Electromagnetic Induction
EM61	EMI-based detection system build by Geonics, Ltd.
EM68	EMI-based detection system build by Geonics, Ltd.
EoDTx120M	Proposed GapEOD UltraTEM Marine high power transmitter
EoDTx50M	GapEOD UltraTEM Marine transmitter
EoDTx200	GapEOD terrestrial transmitter
ESTCP	Environmental Security Technology Certification Program
GapEOD	Gap Explosive Ordnance Detection
GPS	Global Positioning System
IGBT	Insulated-Gate Bipolar Transistors
IMU	Inertial Measurement Unit
ISO	Industry Standard Object
ISS	Informed Source Selection
LISO	Large ISO (105mm projectile surrogate)
MEC	Munitions and Explosives of Concern
MATLAB	"MATrix LABoratory", a software package from Mathworks
MISO	Medium ISO (60mm mortar surrogate)
MMF	Magnetomotive force
Mode 1C	a single-transmitter, 25 Hz repetition rate mode for GapEoD transmitters
Mode 1E	a single-transmitter, 75 Hz repetition rate mode for GapEoD transmitters
MOSFET	Metal–oxide–semiconductor field-effect transistor
MPTx500	GapEOD terrestrial transmitter
MR / MM	Munitions Response Program Area project designators for SERDP and ESTCP, Munitions Response
MTA	Marine Towed Array
MOSFET	Metal–Oxide–Semiconductor Field-Effect Transistor
NRL	Naval Research Laboratory
RMS	Root-Mean-Square
ROV	Remotely Operated Vehicle
Rx	Receive
R/V	Research Vessel
SERDP	Strategic Environmental Research and Development Program

Acronyms (Cont.)

SNR	Signal to Noise Ratio
SubTEM	EMI system built by BTG / GapEOD for Boskalis
SubTEMROV	ROV version of the SubTEM
TEMTADS 2x2	Cart-based AGC EMI system developed by NRL
TOI	Target of Interest
Tx	Transmit
T-Cube	Triaxial EMI receiver cube built by GapEOD
UltraTEM	High-powered AGC EMI family of systems from GapEOD
UltraTEMA(4)	An underwater AGC system from TetraTech / BTG / GapEOD
UXO	Unexploded Ordnance
UXOLab	A UXO detection / classification processing software package from BTG
XLISO	Extra-Large ISO (155mm projectile surrogate)
1PPS	A once-per-second timing pulse generated by positioning systems such as GPS

Objective

The combination of unfriendly survey conditions and technology gaps currently prevent routine, systematic detection and classification of underwater, unexploded ordnance (UXO). A 2007 Strategic Environmental Research and Development Program (SERDP) and Environmental Security Technology Certification Program (ESTCP) sponsored workshop [1] identified several high-priority capability and technology gaps in underwater UXO detection and classification, including improving classification results for UXO. This project addresses several of these gaps. Recent efforts have demonstrated that advanced geophysical classification (AGC) techniques can function successfully in a marine environment as well as they do on land. If successful, we will transfer these efforts into a robust, functioning survey system for dynamic classification of UXO in the underwater environment which will then be available as a tool for DoD to use for evaluation and remediation of munitions and explosives of concern (MEC) issues at underwater sites in the inventory.

Leveraging the lessons learned in ESTCP MR-201610 and with the extensive fielding of the BTG/GapEOD UltraTEM Marine family of systems in Europe, the objective of this project is to integrate a high power, AGC-grade electromagnetic induction (EMI) sensor array in the marine towed array (MTA) platform to provide dynamic UXO classification at standoff distances compatible with the MTA's maneuvering profile through the water.

This report documents the results of our design and testing of proof-of-concept versions of an EMI transmitter and transmitter loop design to confirm the originally proposed transmitter design will meet the requirements for successful classification performance. Initial measurements documented that it was possible to generate the desired factor of eight increase in MMF with GapEOD's transmitter design and transmitter loops of 8-16 turns using the 2m x 1m geometry of the inner transmitter loop layout used in MR-201610 and proposed in the project. We demonstrated in excess of 1100 A·turns during testing.

After discussion with the ESTCP Program Office, a more modest approach was explored, to determine what performance could be achieved without significant electronics redesign and the larger inherent technical risk. Based on the results of the design analysis and testing documented in this report, we recommend proceeding with the fabrication of a prototype of the EODT120M transmitter, for testing and the addition of a new Go / No Go decision point upon completion of that task. The specifications for the corresponding transmitter loops are 7 turns of 8 AWG wire and 9 turns of 10 AWG wire, for the large and small transmitter coils, respectively. The design modifications to convert a EODTx50M transmitter into the proposed EODTx120M transmitter are small, understood, and the technical risk manageable.

Technical Approach

Marine Towed Array (MTA)

The MTA is a unique, 4.6 m wide, underwater sensor platform that was developed and successfully demonstrated at multiple marine venues in support of past SERDP and ESTCP projects beginning in 2004. The MTA platform operates as an underwater, flying-wing style towed sensor array. It was originally outfitted with both marine electromagnetic and marine magnetic sensors for detection and mapping of underwater UXO. Recently the EMI sensor array was upgraded from the original technology in ESTCP Project MR-201610. Field testing of the new array in MR-201610 provided proof-of-principle evidence that AGC-grade EMI systems can collect the quality of EMI survey (dynamic) data required to support classification in marine environments. However, the advanced EMI system selected for MR-201610 ultimately was unable to generate sufficient transmit moment to support detection and classification over the entire range of target sizes of interest for munitions response in marine environments.

Fabrication, testing, demonstration, and analysis of the MTA were conducted under ESTCP Project MM-0324 [2,3]. The sensor platform is shown in Figure 1. The original EMI sensor system was based on the Geonics Model EM68. It failed during demonstration testing. In MR-201610, the single transmitter coil and receiver coils from the EM68 were replaced with an overlapping rectangular transmitter loop design where a large main loop (green), and two inset, inner loops (blue) were installed, shown schematically in Figure 1 (right) fabricated from 20 turns of 14 AWG stranded wire. The system was equipped with 6 triaxial receiver cubes, like those used in the TEMTADS 2x2 (MR-200909), orange ovals. Using a cDAQ system from G&G Sciences, a current of 5.7 A could be generated in the outer loop with typical AGC dynamic survey settings.

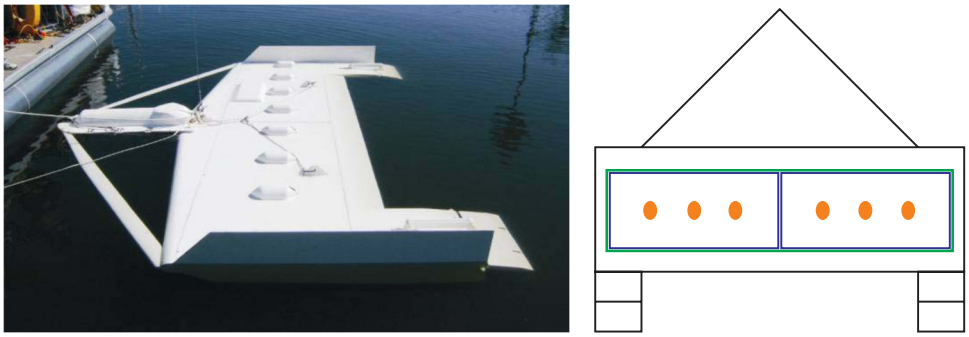

Figure 1. MTA: (left) completed sensor platform, (right). Upgraded EMI array from MR-201610

The MTA platform was originally towed by a triple-hull pontoon boat, which was serviceable but limited in towing performance. During MR-201610, a generic tow point was developed which allows easy installation of the MTA on research vessels (*R/V*) of opportunity.

Wing attitude (yaw, pitch, and roll) and altitude (or depth) are controlled by an autopilot computer operating on the tow vessel. Inputs to the autopilot include a tactical-grade inertial measurement unit (IMU) and altitude and depth sensors mounted on the wing. After system upgrades and modifications to the original MTA in 2011 during an investigation in and around the San Diego Harbor shipping lanes [4], the operational depth capability was increased to greater than 65 ft. Auxiliary cabling and plumbing implemented for MR-201610 currently limits the operational depth of the array to ~30 ft. The proposed effort will resolve this limitation.

UltraTEM

The Black Tusk Geophysics (BTG / Gap Explosive Ordnance Detection (GapEOD) UltraTEM system, a multi-component, multi-sensor system that uses time-domain EMI to detect and characterize buried metal, can be deployed for both terrestrial and marine applications. The system has proven its unique capabilities in European-based production surveys for large area MEC detection, deep large MEC detection, detection of ground-engaging tools in mine stockpiles, and clearance of harbors before dredging. The UltraTEM Marine system has been used extensively with BTG and GapEOD's partner Boskalis, for support of harbor dredging projects in Portsmouth and Dover Harbors in the United Kingdom. The photo below shows the 6 m x 9 m sledge that was built by Boskalis, to house a 5-transmitter by 28-receiver cube underwater sensor that was named the "SubTEM," shown in Figure 2. A five transmitter towed-array variant of the system was successfully validated for terrestrial, one-pass classification at Aberdeen Proving Ground (APG) through the DoD AGC Accreditation Program (DAGCAP) in August 2019.

Figure 2. BTG/GapEOD/Boskalis SubTEM. For the Portsmouth project the SubTEM system was deployed on a sledge that was dragged over the sea-bottom

The UltraTEM system is comprised of the following five components:

1. A high-current transmitter connected to multiple transmitter loops mounted to the detection system. The marine system comes in variants with either 1 or 5 transmitter drivers per enclosure;

2. Multiple three-component receiver sensor "T-cubes" comprised of three orthogonal coils with dimensions of 15cm x 15cm x 15cm each. These sensor cubes are then connected to receiver cube enclosures which can support up to 6 sensor cubes.
3. A submersible power supply with a wide AC input range (90 to 260 V) and variable DC output of up to 50 Amps at 30 volts. The power-supply is used to provide power for both the receiver and the transmitter enclosures. Based on our initial testing, the transmitter and power supply will have to be uprated to reach the transmit moment goal of 800 A·turns.
4. An UltraTEM data acquisition system (DAQ) running proprietary BTField software.
5. A position and attitude system for determining the precise location and orientation of the receivers.

The UltraTEM represents a next generation EMI sensor that, when appropriately configured and deployed, provides AGC capabilities. The UltraTEM has a number of unique characteristics when compared to sensors developed and deployed by other UXO firms for AGC including: (1) support for large transmitter coils (*i.e.*, 1.8m x 1.8m) and high transmitter dipole moment (*e.g.*, 300 A·turns for the SubTEM marine system); (2) custom configurability with multiple transmitter loops and sensor cubes to address specific applications and environments; (3) extremely rugged and reliable electronics with precision time synchronization of all sensor streams to the 1pulse per second (1PPS) signal from an integrated GPS receiver; and (4) integration with the BTField software, which can be easily custom configured with new transmitter receiver geometries and used for near real-time processing and interpretation of the collected data. The UltraTEM electronics and power supply enclosures are pictured in Figure 3. An example receiver T-cube is shown in Figure 4.

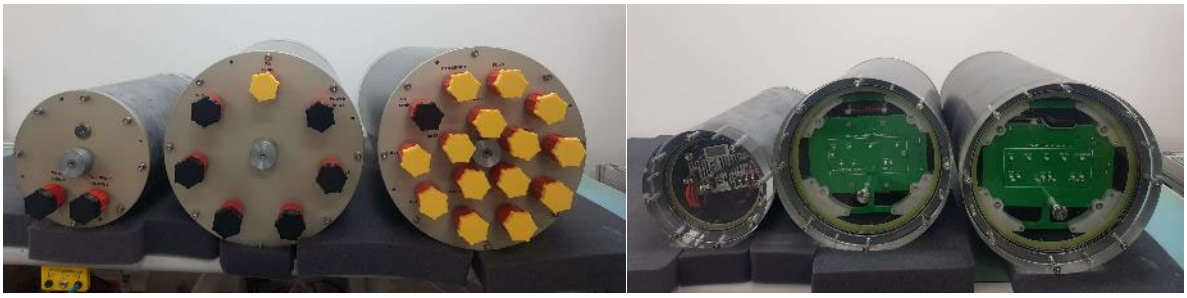

Figure 3. UltraTEM enclosures (from left to right: power supply, transmitter, and receiver)

Figure 4. UltraTEM T-Cube receiver assembly and integrated cable

UXOLab and BTField

In this project, data will be processed by Black Tusk Geophysics (BTG) using the DAGCAP-validated UXOLab software package and by the NRL team using BTField Classify. The ease of implementation of new functionality and the wealth of flexibility inherent in UXOLab make it the ideal package for test and evaluation of new AGC sensors. Developing UXOLab in the MATLAB environment has meant that advancements made through SERDP-funded projects are readily incorporated into the software where they can be rigorously tested. Key algorithms and capabilities from UXOLab have been ported to BTField software which is well suited to large scale production projects run by industry geophysicists.

The technology transition pathway for the UltraTEM system is through the BTField software. BTField is a real-time data acquisition and classification system for buried metal detection. It has been designed to meet the needs of both data collection crews and geophysicists by allowing processing and inversions to run simultaneously as data is being collected. A data acquisition mode of BTField is shown in Figure 5 for the SubTEMROV system. BTField combines data collection and post-processing capabilities into a single software package. The distributed nature of the BTField infrastructure is well suited to multiple, simultaneous workflows and supports transfer from one installation to another (*e.g.*, from the data acquisition vessel to shore-based analysis personnel and archiving resources. BTField has collected data from a variety of terrestrial and marine EMI sensing platforms ranging from a terrestrial cart sensor with a single transmitter and four receiver cubes to a large marine sled platform with five transmitters and twenty-eight receiver cubes.

BTField was used to collect UltraTEM data at the DAGCAP test site at APG in July 2019 as part of the successful hardware validation of the UltraTEM for one pass classification. Since that time BTG have been working to transfer the DAGCAP validated data processing and interpretation algorithms from UXOLab into the BTField application. A beta release of BTField with Informed Source Selection (ISS) capabilities was rolled out in early August 2020 and has been validated for use in AGC projects by DAGCAP.

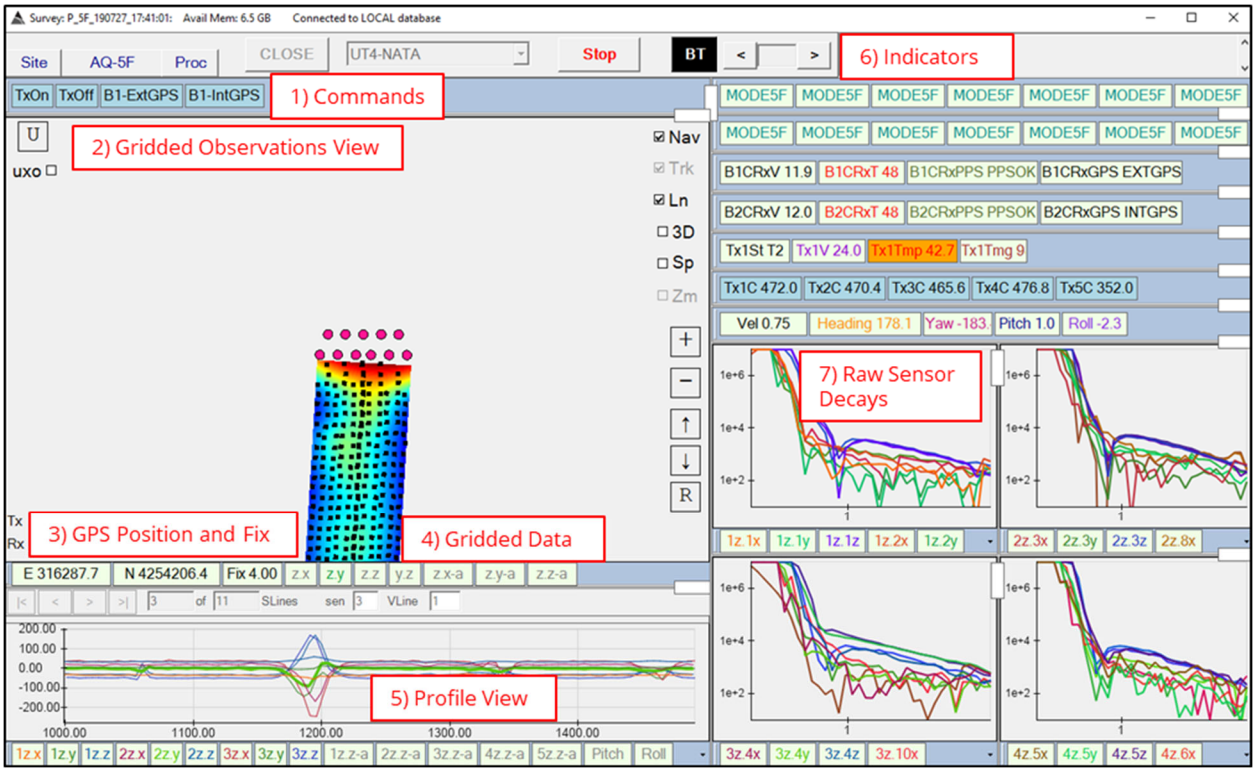

Figure 5. BTField in data acquisition mode for the UltraTEM Classifier system.

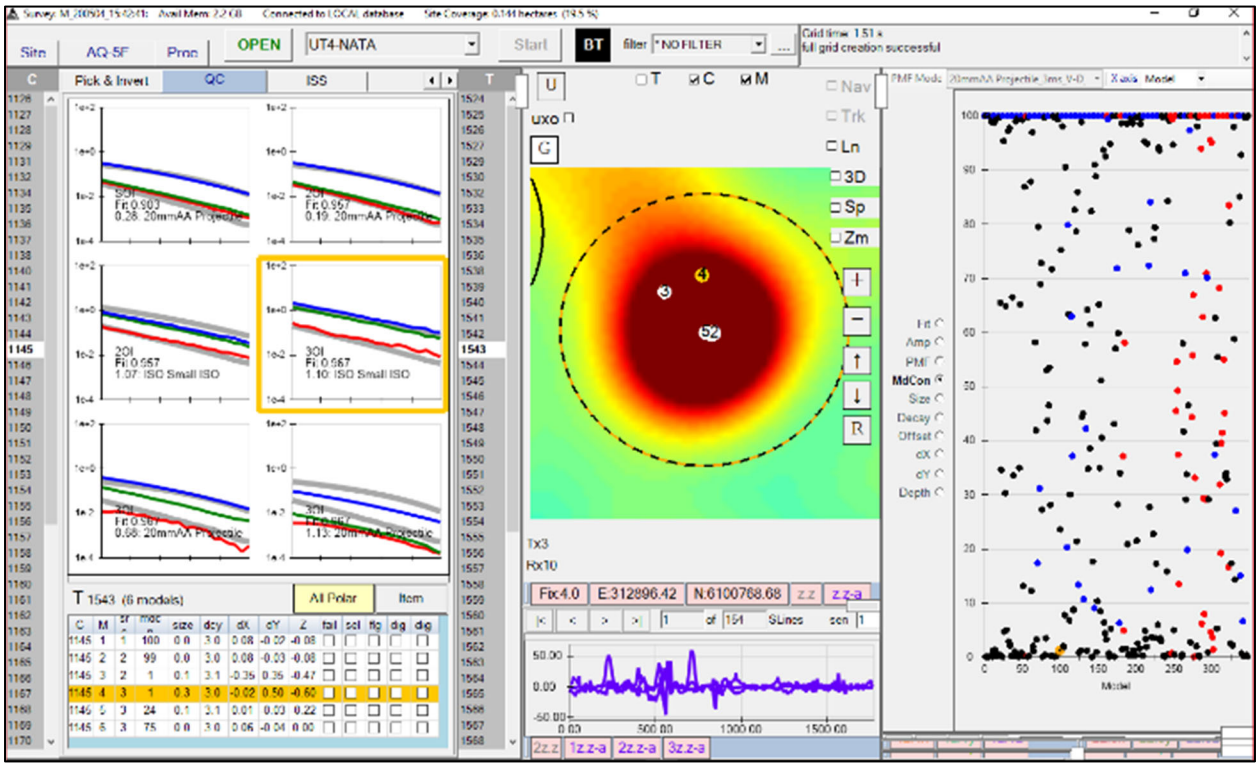

Figure 6. BTField ISS software interface.

Testing and Results

Benchmarking Existing Array

Testing of the MR-201610 EMI Array was conducted at our facilities at Blossom Point on June 18, 2021 to establish a performance baseline against which array performance with the proposed electronics upgrades could be compared. Because of the placement of the magnetometers in the MR-201610 demonstration the receivers were not evenly spaced, leaving a significant gap in the center of the array. The magnetometers will be removed for this project, so we reconfigured the receivers to be evenly spaced in this test. The proposed upgrades are intended to improve performance by about a factor of eight in signal strength with no increase in the noise level. Figure 7 shows the basic test configuration. The array is laid out on top of a six-foot tall wooden platform. Data are collected as a hollow steel ball (6, 8, or 12 inch diameter) rolls along a 16' long wooden rail set up below the array. The 12" ball has a signal comparable to the average signal from a 155mm projectile, and the 8" and 6" balls have signals comparable to the average signals from 105mm and 75mm projectiles, respectively. The picture on the left shows the rail arranged for a transverse roll from right to left (facing forward) under the array. The diagram on the right shows the 8" ball atop the rail in cross-section.

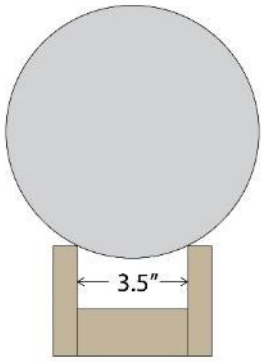

Figure 7. Left: Rail (white) supported on plastic shelves beneath array for side-to-side roll of hollow steel ball. Right: Cross section showing 8" diameter steel ball atop rail.

Transverse rolls of the 8" ball with the rail 58 cm below the coils and 30 cm aft of the array centerline were used for checkout to make sure that all components were working properly and were properly connected. Note that the rail is a bit longer (4.88 m) than the array is wide (4.58 m). Figure 8 shows the z-axis responses of the receivers at 0.216 ms decay to excitation of the 8" ball by the large (outer) transmit loop as the ball is rolled under the array. The plot on the left shows the original receiver configuration, which had to accommodate magnetometer holders in

addition to the receivers. This left a wider spacing between the two innermost receivers (3 and 4) than between the others. The asymmetry in the response at receiver 1 arises as the ball is placed on the end of the rail. The rail is tilted slightly down from right to left (by about 9°), so signals decrease in strength as the ball passes under the different receivers. Tilt was only a couple of degrees in the fore-aft rolls used for signal strength measurements: Just enough to make sure the ball would not stall. Magnetometers will not be included in the new array, which will have the receivers evenly spaced. The plot on the right shows the responses with evenly spaced receivers.

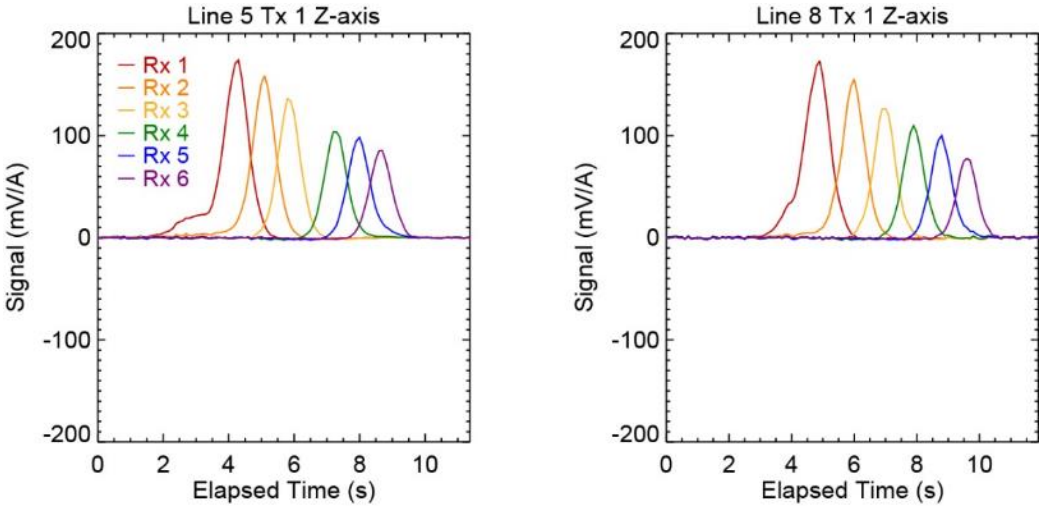

Figure 8. Z-axis response of 8" ball at 0.216 ms decay to large transmit coil excitation as ball rolls beneath the array. The plot on the left shows the original receiver configuration while that on the right is with the receivers evenly spaced across the array.

Signal strength measurements were made with the ball rolling along the rail aligned fore-aft at distances below the array of 38 cm, 81 cm, 125 cm and 171 cm. This simulates the array being towed over a target. The rail was centered between receivers 1 and 2. Figure 9 shows the setup with the rail 125 cm below the array. At 4.88 m, the length of the rail is a good match to the 5 m data stretches typically used for dipole inversion in the 2019 York River demonstrations. The rolling speed (roughly 0.9 to 1.1 m/s) was comparable to the nominal 1 m/s tow speed in the York River tests. Rolling speed was not measured independently. It was determined *post facto* as part of the dipole inversion. Accounting for acceleration and/or rail fore-aft tilt had no significant effect on dipole inversion results.

Signal strength data are shown in Figure 10. The plot on the left shows the peak z-axis response on receiver 2 for the 12" ball excited by the main transmitter loop (circles). The plotted distance below the array accounts for the height of the ball's center above the rail and the thickness of the coils. The crosses are peak z-axis signals over the 12" ball in the York River tests. The data are normalized by the transmit current. In the York River tests the transmit current was 5.7 A, but it was only 4.8 A for the tests at Blossom Point. By controlling the array-target geometry we have a more consistent signal *vs.* range response. The plot on the right shows data and response curves

for all three balls. In this case the signals are not normalized by the transmit current. The RMS noise level is shown by the dashed line. It is some 50% higher than the noise level seen in the York River tests. Checkout data collected on the previous day (June 17) had a noise level lower by about 10% than that shown in the figure. The response curves were calculated using standard dipole response models fit to the test data. The procedure is the same as that used previously to construct EM61 response curves. *Ceteris paribus*, response curves based on MTA data collected using the enhanced (Black Tusk and GapEOD) electronics should be a factor of eight higher relative to the noise.

Figure 9. Setup for baseline signal measurements with the rail aligned fore-aft beneath the array.

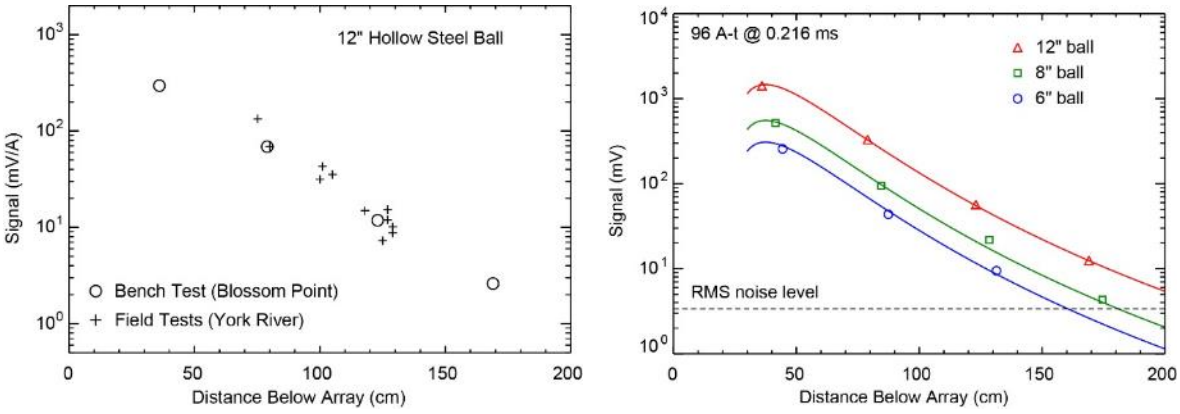

Figure 10. Peak Z-axis response on receiver 2 with outer loop excitation as a hollow steel ball rolls from front to back under the array between receivers 1 and 2. Left: 12" ball response *vs.* depth (circles) measured at Blossom Point compared with peak responses 12" ball measured during York River tests (plusses). Right: Data and response curves for all three balls.

Figure 11 summarizes the classification performance results for an XLISO (6" diameter by 18" long steel pipe section, which serves as a 155mm surrogate) from the York River MTA

demonstrations. The symbols correspond to data from the array crossings over XLISOs. The dashed lines show the range of signal strengths calculated using the standard dipole response model for the range of crossing conditions, and the lower solid curve is their average. The solid symbols represent measurements which had sufficient SNR to classify, while the SNR for the open symbols measurements did not. At a transmit moment of ~110 A·turns, this corresponds to an effective array standoff of 1 m. The upper solid line indicates predicted response curve for an 800 A·turns system, which is predicted to yield a 2m standoff for an XLISO. The horizontal dotted line is provided as a guide for the eye and is placed midway between the solid and open circles, representing a fit coherence of 0.8.

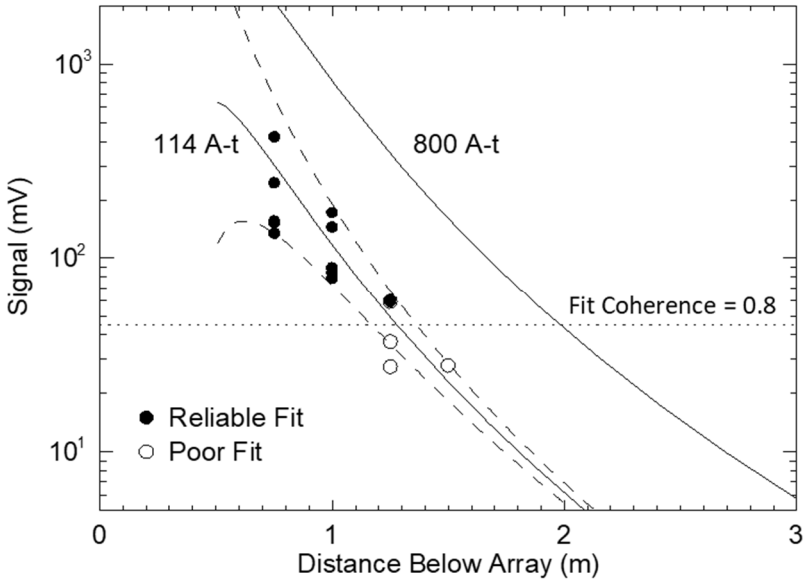

Figure 11. Response curve for an XLISO and the MR-201610 EMI array. Solid symbols are for measurements which had sufficient SNR to classify, the SNR for the open symbols did not. The upper solid line indicates predicted response curve for an 800 A·turns system. The dotted line represents a fit coherence of 0.8.

Comparison of Existing UltraTEM Marine Transmitter to UltraTEM MTA Requirements

As was discussed in the MR-201610 Final Report [5], the target design for the EMI transmitter for this project is a configuration capable of generating ~800 A·turns while not compromising the transmitter turn-off time. The standard UltraTEM Marine AGC system routinely operated at 50 A, having operated in the marine environment for hundreds of hours at 300 A·turns. This system has been recently demonstrated as part of the BTG / TetraTech / GapEOD UltraTEMA4 system demonstration in Washington State [6] as part of ESTCP project MR-5073. The force that sets up a magnetic field within and around an object is termed the magnetomotive force (MMF) and has the units of A·turns. Given the promising results of TEMA4 system so far, an entirely reasonable question is "why does the design of this project target a significantly higher MMF than the TEMA4 requires," or put another way, "what would be the performance degradation of using the standard 300 A·turns?"

To answer these questions, we must look at some of the detailed differences between the two platforms and their deployment. Figure 12 shows the UltraTEMA4 and MTA array configurations schematically traveling along a survey line. Additionally, the magnitude of the primary field for each of the transmit coils along a line 1.5 m below the array and 0.75 m to port (left) of the center of the array. The UltraTEMA4 has four EMI transmitter, three overlapping coils at the front of the array and one larger coil behind the first three. The MTA has three transmitter loops, a large outer loop, and two side-by-side inner loops. The geometry of the MTA wing does not allow for wider or longer transmitter designs, as is. The primary field curves are color coded to their respective transmit coils. The black curves are the averages over all of the transmit coils in each array. Each of the transmit coils in the UltraTEM Marine carry 300 A·turns. The MTA has the proposed 800 A·turns in the outer transmit coil and 1250 A·turns in each of the inner transmit coils. Averaged over the width of the arrays, the peak primary field strength is 47.6 A/m for the MTA and 16.7 A/m for the UltraTEM Marine, so that as proposed the MTA produces primary fields 1.5 m below the array are a factor 2.85 larger than the UltraTEM Marine. Both are towed at a nominal speed of 1 m/s and both operate at 90 Hz. The UltraTEM Marine has 12 receiver cubes, while the MTA has 6. The full width half maximum extents of the averaged fields along track 1.5 m below the arrays are 3.03 m and 2.64 m for the UltraTEM Marine and the MTA respectively, so the UltraTEM Marine samples the target response a factor of (3.03/2.64) x (12/6) = 2.30 more often than the MTA. Roughly speaking, as proposed the increased field strength of the MTA array compensates for the increased sampling of the target response with the UltraTEM Marine.

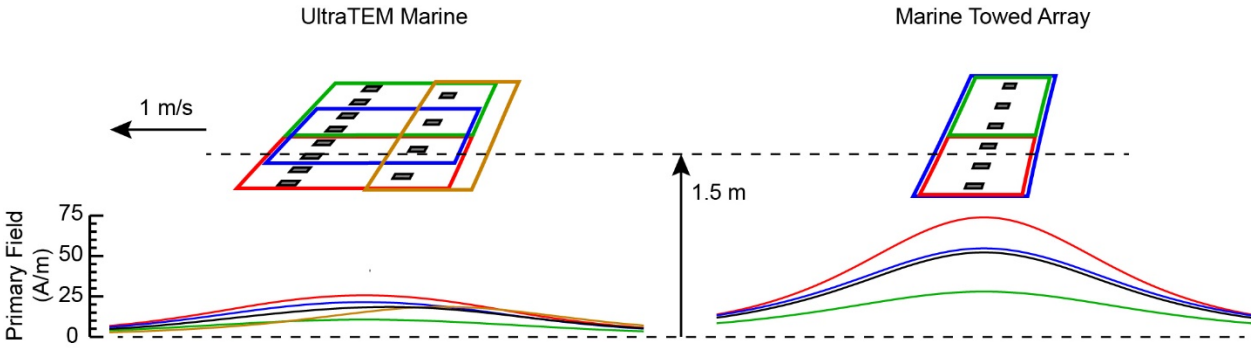

Figure 12. (above) The UltraTEM Marine (TEMA4) and MTA array configurations shown schematically. (below) The magnitude of the primary field for each of the transmit coils along a line 1.5 m below the array and 0.75 m to port (left) of the center of the array.

Further, modeling reported in Appendix B would indicate that an increase in the transmitter current of a factor of 2.5 to 4 would be required to achieve the required stand-off objective.

Bench Testing of Transmitter Design

With the benchmark measurements in hand, we proceeded to bench testing for carrying high currents through a test loop. Initial calculations indicated that for the inner transmitter loops in the design, 2.25 m x 1 m, a 16-turn loop of 4 mm^2 wire would be a good starting point. A high-powered GapEOD transmitter (Model MPTx500) was used (~400 Amp max.), not an UltraTEM marine transmitter (Model EODTx50M, 50 Amp max.), for this testing, as the voltage and

current requirements for this test exceeded the limits on the standard version of that transmitter. The MPTx500 transmitter has a limited set of options for the repetition rate of the transmitter. A repetition rate of 25 Hz, rather than a typical dynamic survey rate (*i.e.*, 75 or 90 Hz) was used. The tests were successful, generated 69 Amperes, or 1,104 A·turns, at 25 Hz with a 50% duty cycle. To accomplish this, the transmitter was operated at ~60 VDC, not the limit of 36 VDC of the standard marine transmitter. The test setup is shown in Figure 13. The current *vs.* time waveform for the transmitter is shown in Figure 14. The time-series shown is of the current passing through the transmitter loop. The average current over an entire second is zero due to the bipolar nature of the waveform. The maximum current achieved and the primary field cutoff time constant of the transmitter determine the size of the secondary fields generated by any metallic objects in the field of view of the receiver.

Figure 13. Bench testing of initial transmitter loop design. (left) Overall setup, (right) Transmitter (Model MPTx500).

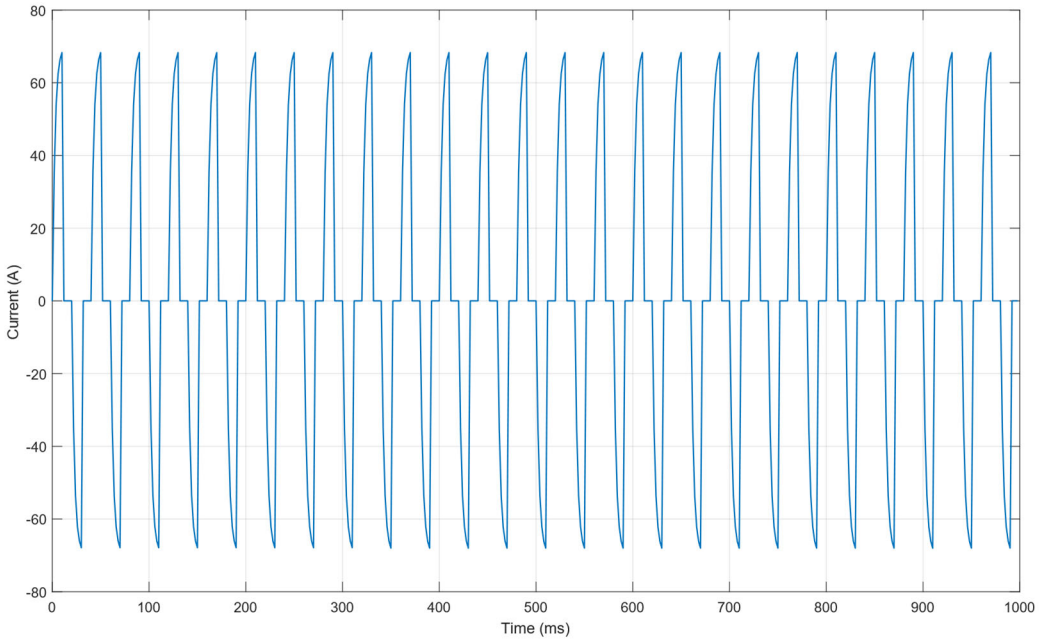

Figure 14. Bench testing – Initial loop current versus time waveform.

Proof-of-Concept Testing of Transmitter Design

Having demonstrated that the desired transmit moment could be generated sustainably, the next tests were to make sure that the transmitter could collapse the magnetic field rapidly enough to collect reliable dynamic data collection (*i.e.*, transmitter shutoff times < 200 μs). Additionally, evaluation of the input voltage requirements and associated issues such as heat dissipation continued in this phase.

These tests were conducted in two phases in a park near GapEOD's facility to allow for careful study of both the signal amplitudes, but the noise floor of the tested configurations as well. Figure 15 shows the field setup. The generator, power supply, and transmitter used for the second phase measurements are shown in Figure 16. Note, as in the bench testing, a high-powered transmitter was used, which is a much larger system physically, and is not indicative of the final transmitter design which will be deployed. In the first phase of testing, the same MPTx500 transmitter as the benchtop measurements was used. This transmitter has a minimum input voltage of 50 V so a section of "feeder" cable had to be connected to increase the resistance of the transmitter loop (otherwise the generated current would have been much higher than our design goal). In the second phase, a later generation transmitter, the EODTx200, was used. It can be operated at higher frequencies and incorporates a number of additional improvements over the older MPTx500 transmitter (*e.g.*, controlled current mode, finer adjustments of current generated).

Figure 15. Proof-of-Concept testing of transmitter loop configurations. Field setup.

Figure 16. Proof-of-Concept testing of transmitter loop configurations. (left) 20 kVA three phase generator, (right) power supply and transmitter (Model EODTx200).

Figure 17. Proof-of-Concept testing of transmitter loop configurations. (top left) 16 turn, 4 mm^2; (top right) 8 turn, 25 mm^2; (bottom left) 12 turn, 6 mm^2; (bottom right) 10 turn, 10 mm^2 coils.

Figure 18 and Table 1 summarize the performance of the four transmitter loop configurations tested. The 25 mm^2, 8 turn loop reaches a maximum current early and then droops prior to turn-off due to the configuration of the electronics in the MPTx500 transmitter. The other configurations all continue charging until the transmitter turn-off, as is desired. Regarding the turn-off behavior of the transmitter, the results are shown in Figure 19 for the first two loops and in Figure 20 for all four loops.

Table 1 – Transmitter Loops Tested. Information on the number of turns and wire cross section as well as the current, power and voltage of each loop at the point of turn-off are provided.

Loop ID	Wire Cross Section (mm^2)	Number of Turns	Current at turn-off (A)	Current x Turns (A)	Input voltage (V)	Power at turn-off (kW)
1	4	16	67.6	1,081	70	4.7
2	25	8	143.1	1,145	79	11.3
3	6	12	100.9	1,211	49	4.9
4	10	10	121.1	1,211	32	3.9

As can be seen in Figure 19, the 8-turn loop turns off faster due to lower inductance. The 8-turn loop has a larger late time response due to the large amount of copper in the transmitter loop. The 16-turn loop takes a very long time to turn off as the inductance is very high. The late time response of 16 turn loop is faster due to a smaller amount of copper being present. These first two coils were wound using available materials and do not represent the material that will be used. Given these results, intermediate gauge wire was acquired and two additional loops were wound, and tested. The results are summarized in Figure 20 and Figure 21. Figure 20 shows the full time decay and Figure 21 focuses on the portion of the time decay that is relevant to for AGC in this context. The second set of loops perform very similarly, with the 12-turn loop being slightly faster to turn on. Both of these new loops demonstrate better early- and late-time response than the first two loops.

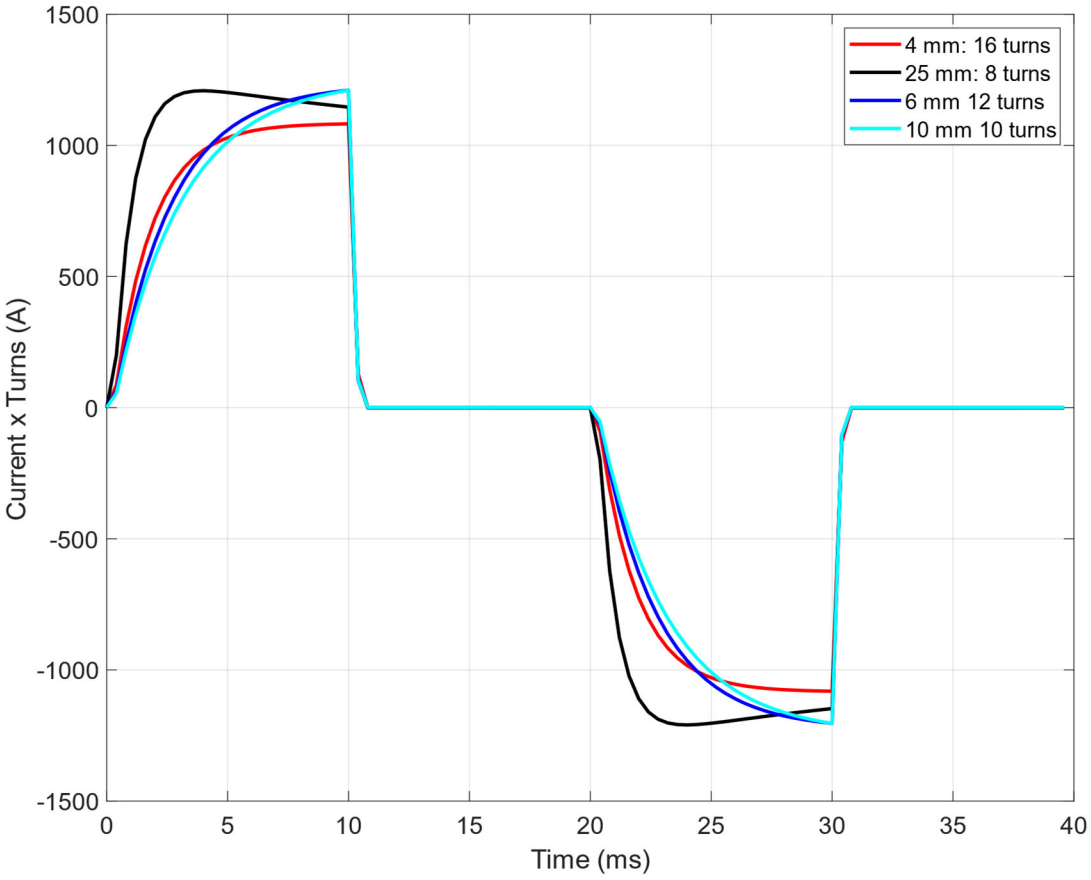

Figure 18. Proof-of-Concept testing of transmitter loop configurations. Transmitter behavior

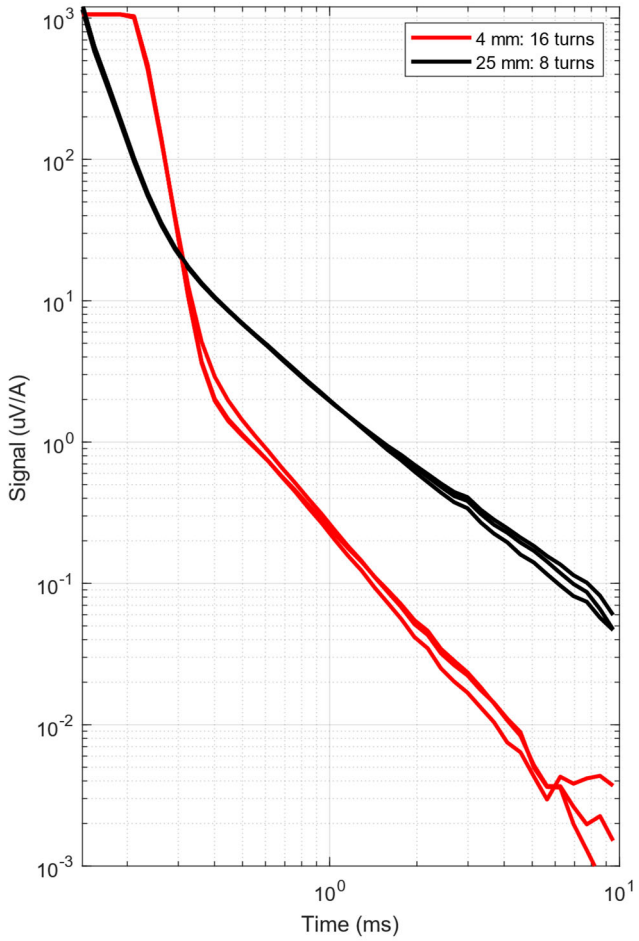

Figure 19. Proof-of-Concept testing of transmitter loop configurations. Turn-off behavior for first two loops for all three receivers (Z-component data).

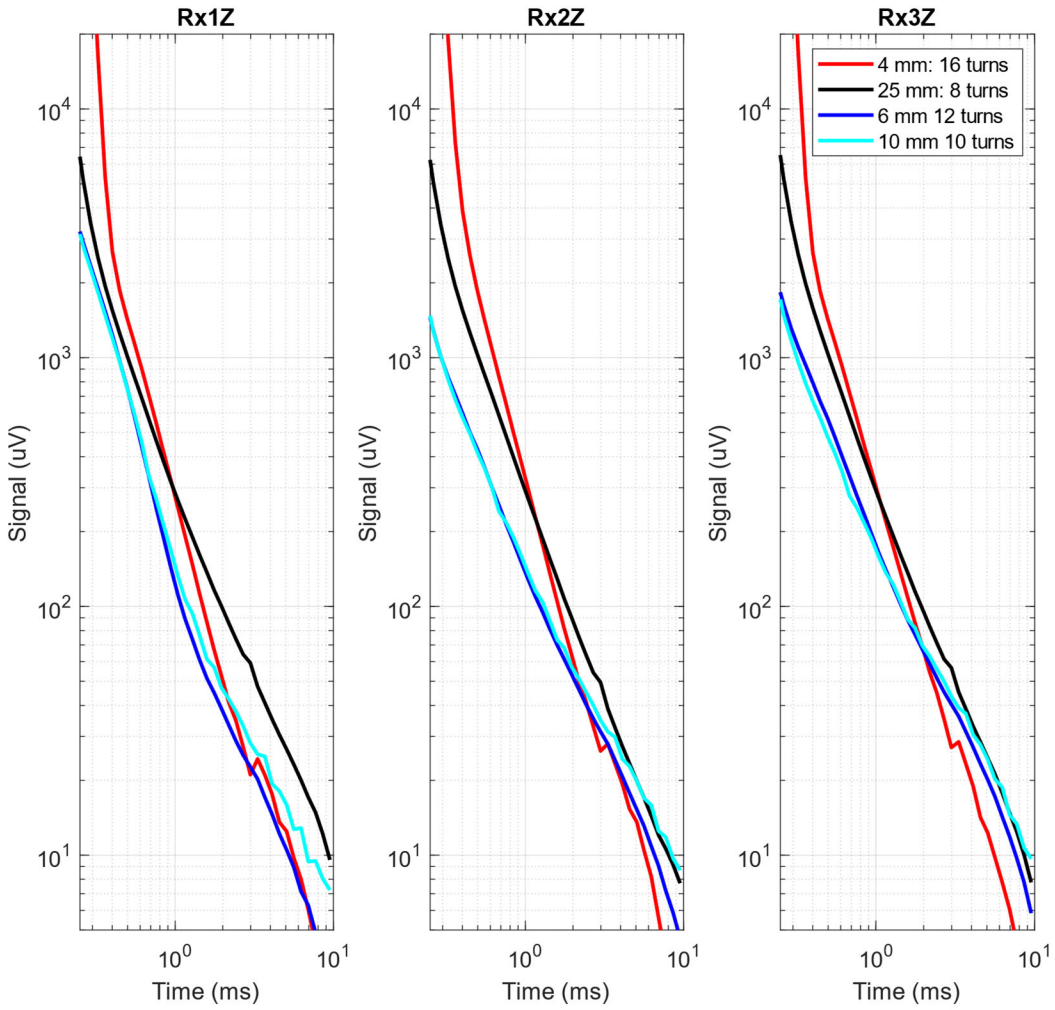

Figure 20. Proof-of-Concept testing of transmitter loop configurations. Turn-off behavior in the Z-component of the three cubes, including early times.

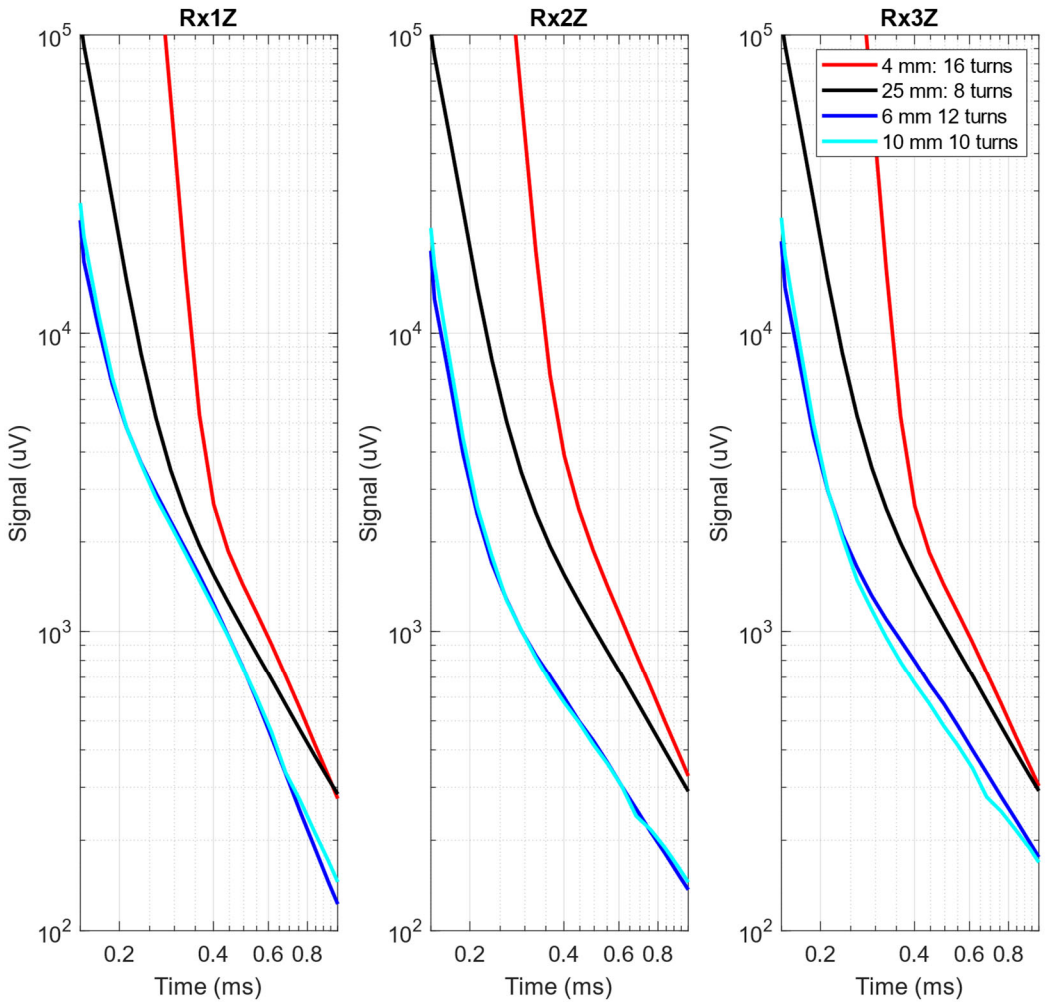

Figure 21. Proof-of-Concept testing of transmitter loop configurations. Classification-relevant decay times turn-off behavior in the Z-component of the three cubes.

Response to Targets

Figure 22 and Figure 23 summarize the response of the test configuration using loop 1 (4 mm^2, 16 turns) and three receivers for a medium ISO (MISO, 60mm mortar surrogate) and a large ISO (LISO, 105mm projectile surrogate) as a function of array – ISO distance (range) and orientation (vertical and horizontal, with respect to the array).

(a) Horizontal medium ISO

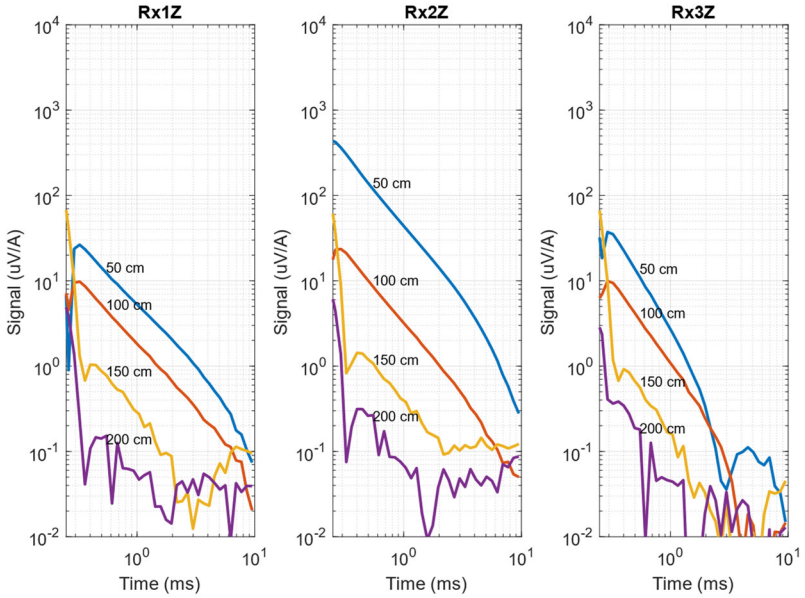

(b) Vertical medium ISO

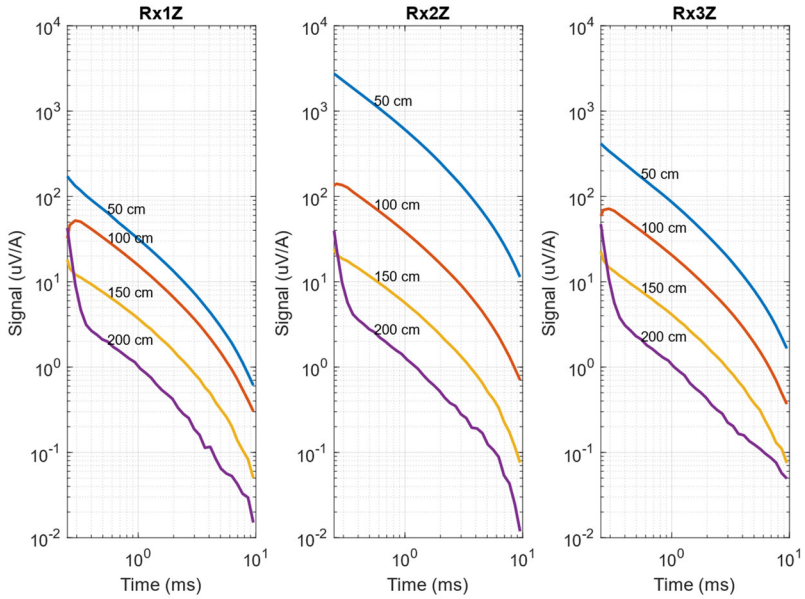

Figure 22. Proof-of-Concept testing of transmitter loop configurations. Medium ISO.

(a) Horizontal large ISO

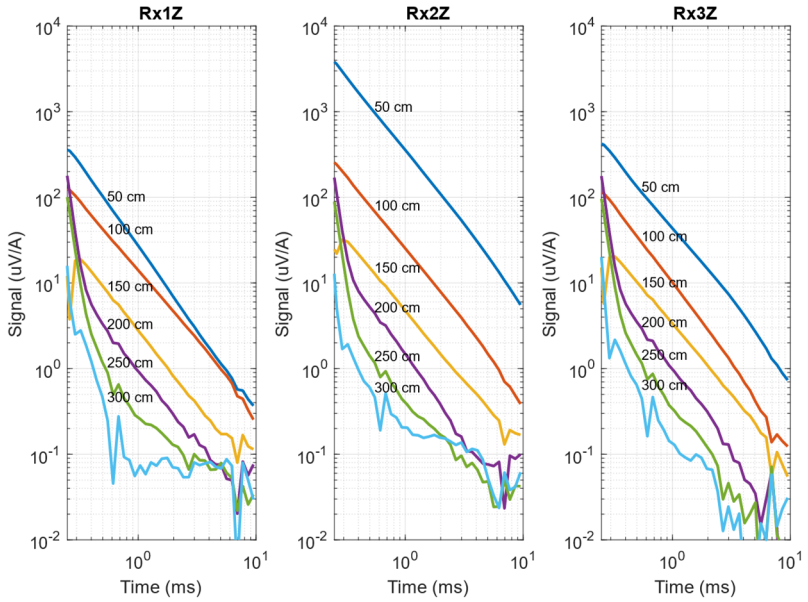

(b) Vertical large ISO

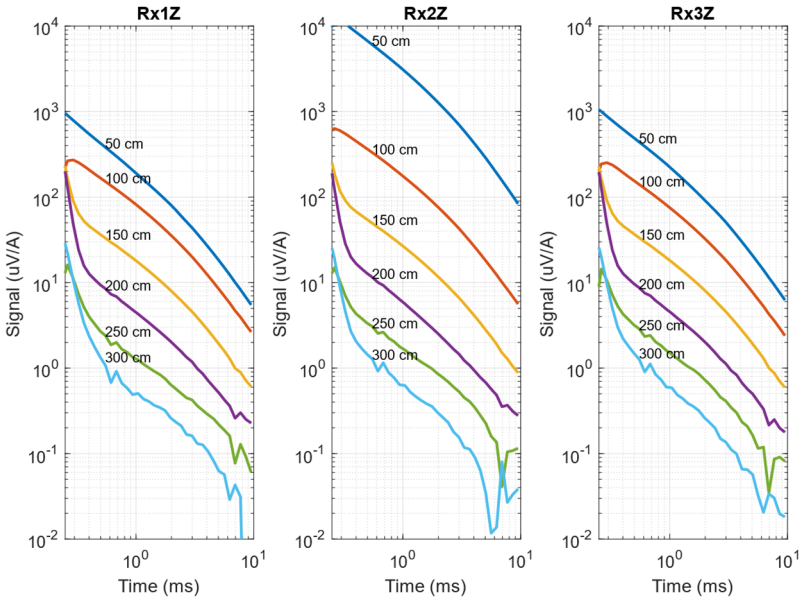

Figure 23. Proof-of-Concept testing of transmitter loop configurations. Large ISO.

Signal to Noise Considerations

Figure 24 compares the early time background response for one of the MR-201610 MTA inner transmitter loops at Blossom Point (loops removed from wing and set on a test stand) in June with the background response measured using loops 1 and 2 in October and loop 4 in November. Loop 1 was slower to turn off. The response from the MTA loop (20 turns) saturates at about 9 V for decay times out to 0.12 ms or so. Loop 1 saturates at just over 1 V for decay times out to 0.21 ms or so, while loop 2 and loop 4 saturate out to about 0.1 ms. All the loops decay reasonably well after the early time saturation.

Figure 25 compares RMS noise levels. The data are differenced to remove the slope then the standard deviation is divided by $\sqrt{2}$. Data for the MTA and BTG loops are plotted in units of microTesla per second because the noise is primarily ambient rather than electronic. Corresponding scales in Volts are on the right. The MTA data are from the noise runs collected on the way back to the dock during the December 2019 tests at the mouth of the York River. There is perhaps a factor of three spread in the noise levels observed in the BTG tests, which is not unreasonable. We have observed significant variations in the noise level from place-to-place and time-to-time. The MTA noise level is a bit higher than the BTG noise levels.

The BTG data were collected at 25 Hz (mode 1C) and 75 Hz (mode 1E) for 50Hz suppression. The MTA data were collected at 90 Hz for 60 Hz suppression. The BTG raw decays were sampled every 1.25 μs and logarithmically gated with an average gate width of 10.5%. The MTA decays were sampled every 4 μs and logarithmically gated with an average gate width of 22.2%. The 10 ms BTG data were collected using mode 1C. Five internal decay pairs (each 40 μs long) are stacked per measurement in mode 1C, with five data values output per second. The 3 ms BTG data were collected using mode 1E. Six internal decay pairs are stacked per measurement in mode 1E, with twelve data values output per second. This means that there are 2.5 times as many noise samples with BTG mode 1C than there are with the MTA data, and 3.0 times as many with mode 1E. Hence, at the same place and time we would expect the MTA noise level to be higher than the BTG noise level: About 58% higher than mode 1C noise and about 73% higher than mode 1E.

Figure 26 shows signals *vs.* range measured by BTG using loop 4, mode 1C for a MISO and a LISO. The targets were oriented transverse to the array and aligned along the centerline of the array. The upper curves and symbols are for the center Rx cube, while the lower curves and symbols are for the outer two Rx cubes. The classification threshold from Figure 11 is about 25 times the RMS noise level. With 10.5% gates the BTG system gets twice as many decay times as the MTA (22.2% gates). However, with 90 Hz base frequency (60 Hz suppression, 3 ms decays) the BTG system would only get one sample every 0.2 s for each Tx in a three Tx array, compared to 0.1 s for the cDAQ MTA data. The two probably wash, so that we would expect that this threshold would also apply for the full array. Based on the noise level for the data in

Figure 26 we would thus expect to be able to detect and classify a 105mm projectile out to a range of about 1.6 m with 10x10mm^2 coils operating at 40 V, producing 1205 A·turns in the inner loops and around 840 A·turns in the outer loop.

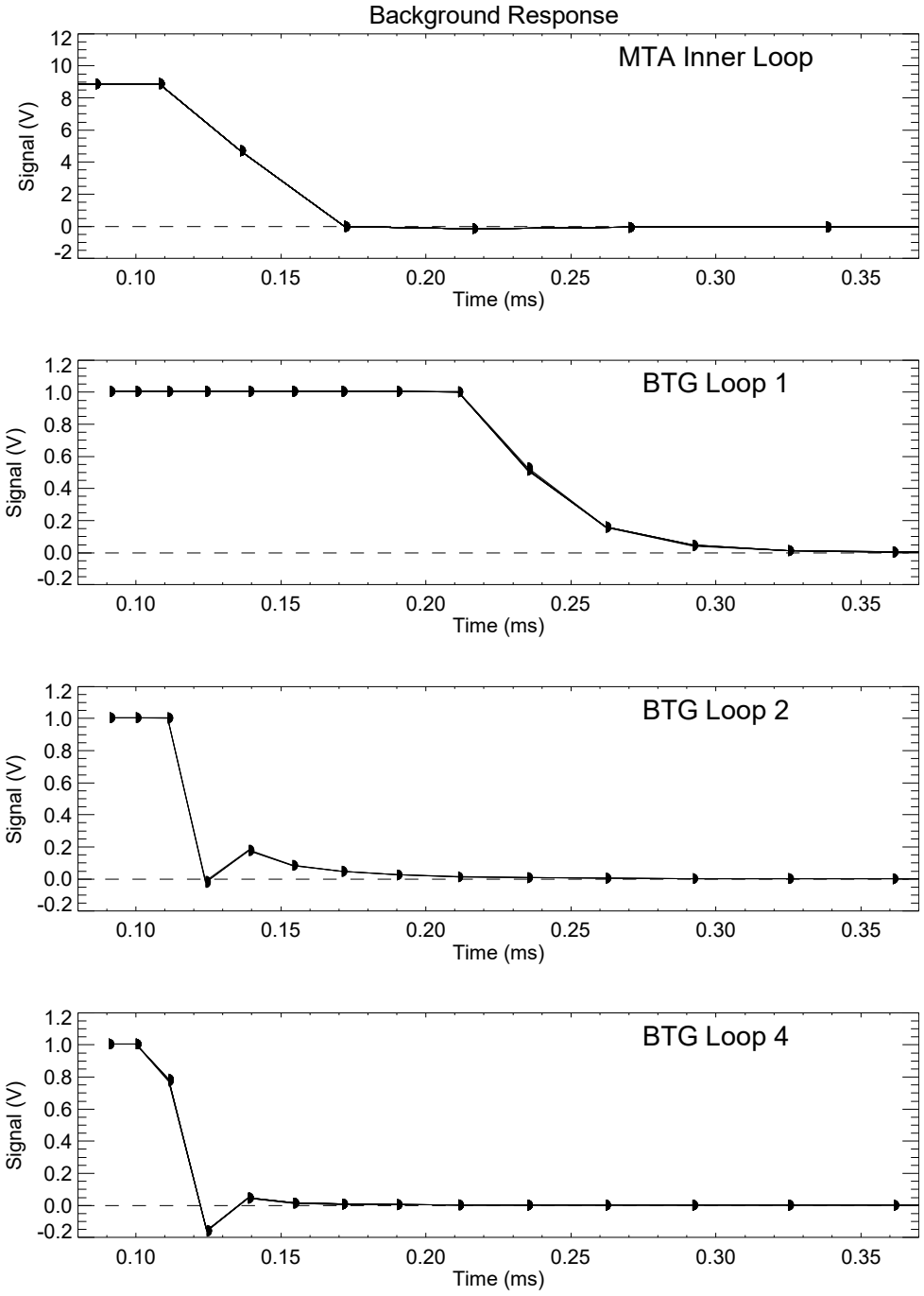

Figure 24. Background Response of loop configurations 1, 2, and 4.

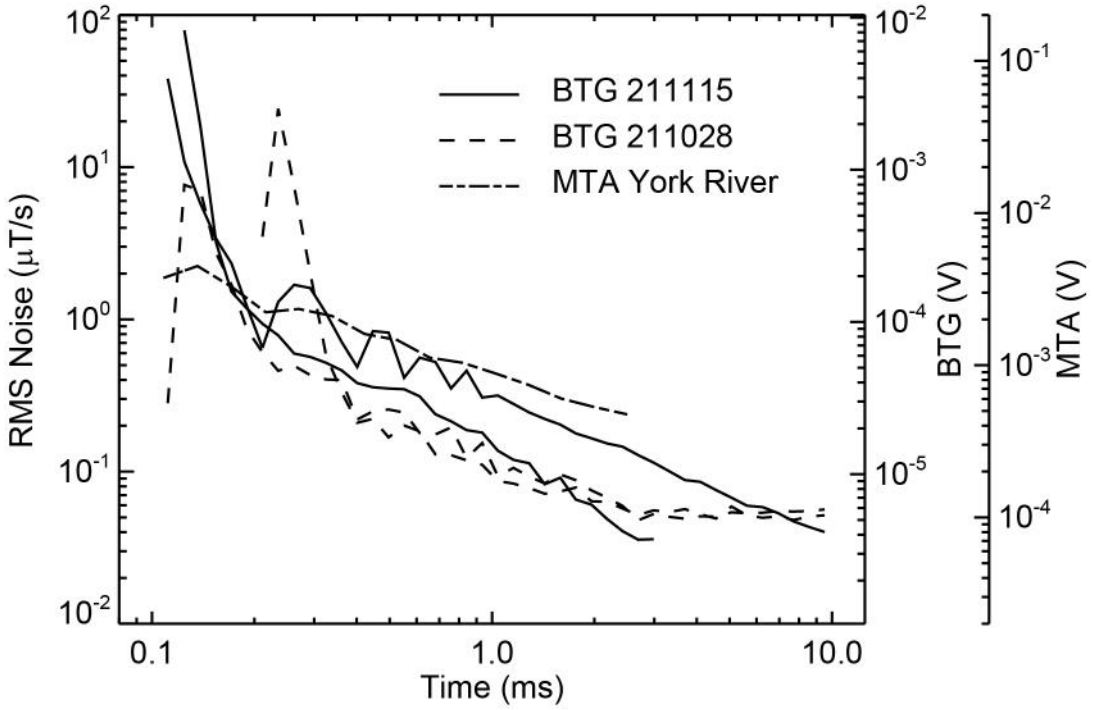

Figure 25. Noise comparison between BTG and MTA data collections. The BTG data was collected in Fall 2021 in a terrestrial setting in Australia. The MTA data was collected in the York River, VA in Winter 2019.

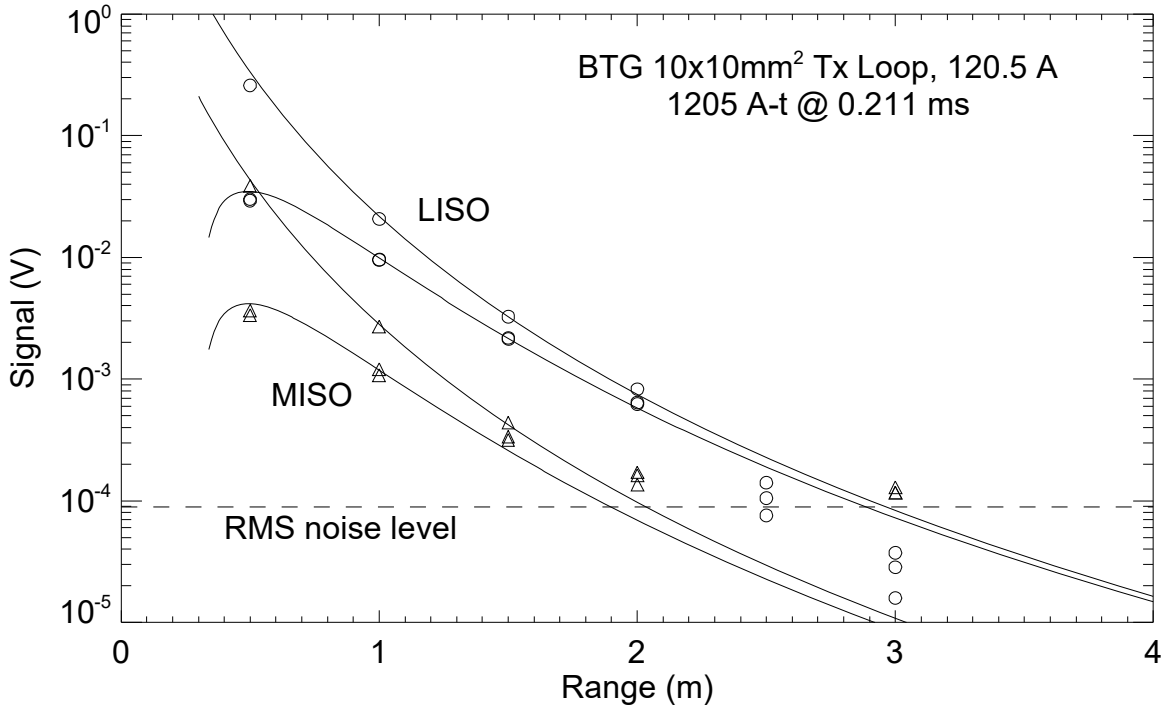

Figure 26. Medium and large ISO signals *vs.* range for BTG loop 4, mode 1C.

An analysis of the noise floor and signal response of the UltraTEMA4 during a shakedown cruise in June, 2021 is given in Appendix B. Figure 25 is updated as Figure 36 to overlay all of these sets of data. The Ostrich Bay, WA UltraTEMA4 noise levels were comparable.

Proposed UltraTEM Marine Transmitter Modifications

The original goal of this project was to reach an 8-fold increase in MMF, as was discussed above. However, in discussions with the ESTCP Program Office it became clear that the inherent technical risk in aiming for these levels (800 and 1250 A·turns) was higher than originally estimated and unacceptable. A design review was conducted by GapEOD's team including their Chief Engineer to evaluate how close to these metrics a transmitter could be built based on the existing design and more controlled technical risk. The analysis results are presented in Appendix A. A factor of 6 larger MMF (700 and 900 A·turns, for the large and small transmitter coils respectively) is achievable with a component-for-component swap on the high-speed switches used in the transmitter and increasing power supply from 1500 to 3000 Watts. This may require moving the power supply from the current enclosure to the slightly larger design currently already used for the transmitter. No changes to connectors are anticipated. Modeling and field data from the UltraTEM4 of the thermal performance for the transmitter heat sink indicates that the existing heat sink should be sufficient. If in prototype testing, this is found not to be true, two simple strategies for mitigation are outlined with low technical risk involved. Appendix A also outlines the specifications for the corresponding transmitter loops, which would be 7 turns of 8 AWG, and 9 turns of 10 AWG, for the large and small transmitter coils respectively. Based on the detection modeling described in Appendix B, the proposed MTA design with the improved transmitter would provide a signal voltage/RMS noise voltage ratio of at least 11.5 at a 2.25 m standoff for a 105mm projectile.

Proposed Milestone and Schedule Modifications

A prototype of the transmitter will be assembled and tested at GapEOD's facilities in Australia. This is an added task, and will have an associated new Go / No Go decision point. Based on parts lead times and assembly time at GapEOD, we would propose this task be scheduled for completion 12 weeks after permission to proceed is received from the Program Office, or roughly May 13, 2022. This roughly coincides with the existing task, "1.5 Test Stand Evaluation of EMI Array and Electronics," scheduled for completion on 03/31/2022. Assuming that this next Go / No Go decision point is successfully passed, again based on parts lead times and assembly time, completion of Task 1.5 would be postponed 8 – 14 weeks further, or to mid- to late August, 2022. All other remaining tasks would be moved back the same amount. Some of the work leading up to Task 1.5's completion, namely the fabrication and check out of the receiver electronics and receiver cubes is not dependent on the results of the transmitter prototype work. If acceptable to the Program Office, this work could be started in parallel with the new task, and potentially bring Task 1.5 to completion earlier.

Proposed Project Cost Ramifications

Adding the proposed prototyping task will incur some additional cost. A ROM estimate is $55,000, primarily for labor. The prototype will have to be assembled and tested by GapEOD and the results evaluated by team members. Once complete, the team will prepare an interim report for the ESTCP Program Office with the results and a recommendation on the new Go / No Go decision point. Additional details on cost will be provided to the Program Manager under separate cover when appropriate.

Conclusions

The EMI array from MR-201610 was removed from the MTA and test stand measurements were made under controlled conditions to ensure that the performance observed during the field tests of MR-201610 could be reliably used to predict the performance metrics for the array to be designed and built in this project. Additionally, the precisely controlled target – array geometries of the test stand measurements will provide valuable benchmark data for comparison during the testing of the new array.

A series of four potential transmitter coil designs were tested at GapEOD's facilities using available transmitters and power supplies. Initial measurements documented that it was possible to generate the desired factor of eight increase in MMF with GapEOD's transmitter design and transmitter loops of 8-16 turns using the 2m x 1m geometry of the inner transmitter loop layout used in MR-201610 and proposed in the project. We demonstrated in excess of 1100 A·turns during testing. Further testing demonstrated that some care is required to achieve a well-damped, rapid turn off for a transmitter loop carrying a large current.

After discussion with the ESTCP Program Office, a more modest approach was explored, to determine what performance could be achieved without significant electronics redesign and the larger inherent technical risk. Based on the results of the testing documented in this report and the design analysis presented in Appendix A, we recommend proceeding with the fabrication of a prototype of the EODT120M transmitter, for testing and the addition of a new Go / No Go decision point. Comparison of the designs and performance between this design and the existing UltraTEMA4 array indicate that the existing EODTx50M transmitter will not support the requirements of the proposed MTA system without some modifications. Appendix A also outlines the specifications for the corresponding transmitter loops, which would be 7 turns of 8 AWG yielding 700 A·turns, and 9 turns of 10 AWG yielding 900 A·turns, for the large and small transmitter coils respectively. As discussed in Appendix A, the design modifications to convert a EODTx50M transmitter into the proposed EODTx120M transmitter are small, understood, and the technical risk manageable. Based on the detection modeling described in Appendix B, the proposed MTA design with the improved transmitter would provide a signal voltage/RMS noise voltage ratio of at least 11.5 at a 2.25 m standoff for a 105mm projectile.

Literature Citations

1. “SERDP and ESTCP Workshop on Technology Needs for the Characterization, Management, and Remediation of Military Munitions in Underwater Environments,” Final Report, October 2007.

2. “Marine Towed Array Technology Demonstration Blossom Point Research Facility,” Final Report, August 2009.

3. “Marine Towed Array Technology Demonstration at the Former Naval Duck Target Facility,” Final Report, November 21, 2005.

4. "Report on the Marine Towed Array Survey of Selected Sites at San Diego Bay," Science Applications International Corporation Technical Report to PWS - R029 by SPAWAR Systems Center, Pacific (SSC-Pacific), June 2012.

5. Marine Towed Array, Underwater EMI Sensor Platform for Metallic Item Detection, ESTCP MR-201610, Final Report,” T.H. Bell, G.M. Massey, G.R. Harbaugh, and D.A. Steinhurst, April, 2020.

6. “UltraTEMA-4 Marine Towed System For Detection and Characterization of Buried Ordnance,” S.B. Billings, R. Funk, and J. Gamey, SERDP / ESTCP Symposium, Washington, DC, December, 2021.

Appendix A: Proposed UltraTEM Marine Transmitter Modifications

Modifications would be needed to be made to the standard EODTx50M marine transmitter to generate the currents required to achieve the desired 800 and 1,200 A·turn goal for the large, outer and smaller, inner transmit coils respectfully. GapEOD could build a transmitter that would meet these desired specifications. In the interests of minimizing the impact on the schedule and budget, GapEOD's senior engineer undertook a design study to determine if some modest changes to the existing EODTx50M transmitter could achieve a significant fraction of the required A·turn objectives. Figure 27 compares block diagrams of the existing EODTx50M transmitter to a proposed EODTx120M variant that reuses most of the existing EODTx50M circuitry.

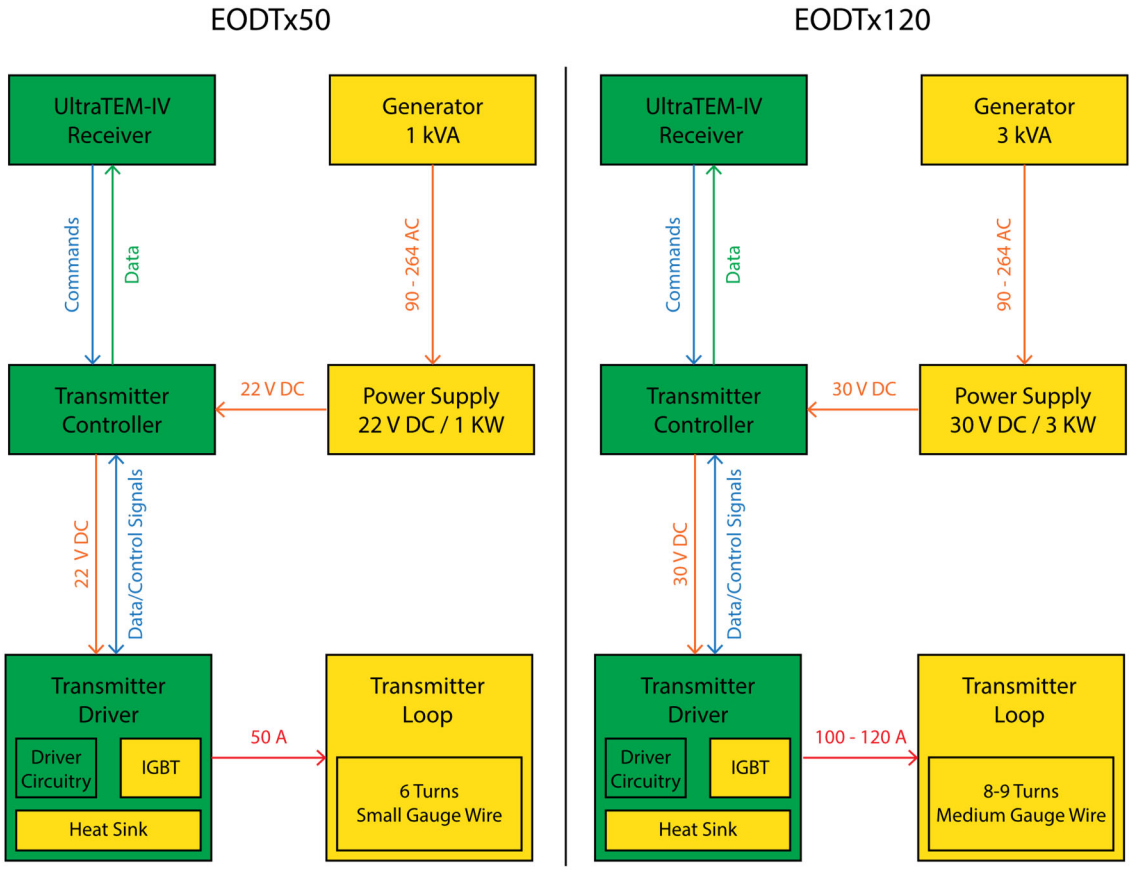

Figure 27. Block diagrams comparing the existing EODTx50M transmitter with the proposed EODTx120M transmitter. Parts of the system that will change are colored yellow.

The resultant configuration is expected to support 700 and 900 A·turn in the large and small loops respectively. These correspond to 87.5% and 75% of the original project objectives.

Blocks shown in green are common between the two transmitter designs, while blocks in yellow show components or subsystems that would need to be modified.

Below we summarize the characteristics and changes required to achieve the 700 / 900 A·turn configuration.

Small coil-design

Small loops (x2) - nominal specifications:

- A·turn specification: 900;
- Size: 2.25 m x 1 m;
- 9 turns;
- Current: 100 A;
- Wire Gauge: 10 AWG (5.26 mm^2);
- Inductance: 400 µH. Inductance is intended to be a conservative estimate (high) but will vary with wire spacing, etc.;
- Resistance: 0.222 Ω;
- Wire length: 58.5 m;
- Resistance per metre: 3.80 mΩ;
- Turn ON time constant: 1.8 ms. To calculate the turn-on time, the loop can be modelled as an RL circuit with an exponential time-constant of L/R.
- Turn OFF time: 40 – 100 µs dependent on clamping voltage used (see discussion in the IGBT section for some considerations regarding turn-off time.

Large coil-design

Large Loop (x1) - nominal specifications:

- A·turn specification: 700;
- Size 4.5 m x 1 m;
- 7 turns;
- Current: 100 A;
- Inductance: 430 µH;
- Wire Gauge: 8 AWG (8.37 mm^2) with a resistor in series to match the resistance of the small loop
- Resistance: 0.222 Ω;
- Wire length: 77 m;
- Resistance per metre: 2.88 mΩ;
- Turn ON time constant: 1.9 ms;
- Turn OFF time: 40 – 100 µs dependent on clamping voltage used;

Notes regarding loops and maximum current generated:

- At an operating frequency of 30Hz the exponential current rise will reach 99% of maximum;
- At an operating frequency of 90Hz the exponential current rise will reach about 78% of maximum;
- The voltage drop across the transmitter output semiconductors will be between 6 and 8 volts depending on the devices chosen. In past versions of the transmitter, the voltage drop has been 6 – 8 V, and it is predicted to be in this range for the new transmitter. As an additional note, there are other components in the output circuit than the MOSFETs that contribute to the total, final voltage drop; and
- The loops will require 100 Amps to be passed through the transmitter connectors which is double the 50 A used with the existing EODTx50M transmitter. We will retain the same connectors but will split the current into two paths and use two connectors per loop. This means that a total of six connectors for three transmitters will be required compared to the five used with five transmitters with the EODTx50M. There is ample space on the faceplate of the transmitter enclosure to accommodate the single extra connector.

Generator

The system will require a peak power output of 100 Amps x 30 V = 3,000 W. This power can be obtained through a single phase 3 kW generator with an input AC voltage of between 90 – 264 V compared to the existing 1 kW single phase generator used with the EODTx50M transmitter. This part of the system will be installed on the vessel. As the transmitters operate in a 50% duty cycle mode the average power consumption will be half the peak consumption (so 1,500 W).

Power Supply

The power-supply converts the single-phase AC power to 30V DC with a maximum output of 100 Amps, compared to the existing power-supply with a 1 kW, 50 Amp maximum that typically operated at 22 V (XP Power model HDS1500PS30[1]). The XP Power model HDS3000PS30[2] is a potential power supply that meets the new required specifications. For comparison, the dimensions of the HSD1500PS30 and the HDS3000PS30 are 294.5 x 63.5 x 127 mm and 366 x 127 x 127 mm, respectively. The proposed unit is roughly 60mm longer and taller, with the same width. The larger size of the 3 kW power supply will require a slightly large enclosure to used.

[1] https://www.xppower.com/portals/0/pdfs/SF_HDS1500.pdf
[2] https://www.xppower.com/portals/0/pdfs/SF_HDS3000.pdf

Transmitter controller and driver circuitry

The transmitter controller and driver circuitry would not change as the existing circuity has been used for transmitters with outputs in the range from 10 to 500 A.

High speed switches

The devices used in the high current switching circuitry will need to be upgraded to improve the turn-off time characteristics of the loops. For the EODTx120M transmitter, they would be either Insulated-Gate Bipolar Transistors (IGBT) or metal–oxide–semiconductor field-effect transistor (MOSFET) devices. The turn-off characteristics of the loops can be modelled as a linear ramp with a time-constant equal to L * I / V (inductance x current divided by the turn-off clamping voltage). The turn off clamping voltage will be between 500 volts and 1600 volts depending mainly on the instantaneous power dissipation capabilities of the chosen/available output devices. Many electronic parts are scarce at the present time. An example of a suitable output device is the Wolfspeed CAB006M12GM3 which has a maximum operating voltage of 1,200 V and maximum continuous output current of 200 A. This is a higher maximum voltage than the MOSFET currently used in the existing EODTx50M, the STMicroelectronics STGE200NB60 device with 600 V and 150 amps continuous current. This device could theoretically provide a clamping voltage of 2,400 V by connecting two of these devices in series (one on each side the loop). Past experience has shown that it is unwise to exceed two-thirds of the maximum clamping voltage providing a sustainable clamping voltage of 1600V (800V x 2) and a turn-off time of approximately 40 μs.

Heat-sink

The size of the heat-sink in the EODTx120M transmitter would need to increase slightly to allow for the increased heat dissipation from operating at 100 A. The existing heat-sink in the EODTx50M is slightly oversized and efficiently cools the transmitter interior when the system is submerged in water. Figure 28 shows a CAD model of the hexagonal heat-sink used for the existing EODTx50M Marine transmitter. There is a transmitter controller on one face and transmitters on five of the size faces. The heat sink is attached to an aluminum face plate that is in contact with the water with fans used to circulate air through the central cavity. Assuming each transmitter generates 50 Amps at 30 V, there's a peak heat generation of 1,500 Watts. But each transmitter is only on for 50% of the time during that transmitter's allotted cycle time which comprises only 20% of each second. This means that the transmitter is only on for 10% of each second so that the average power generated is 150 Watts. Assuming an outside water temperate of 20 ºC, we modelled the rise in temperate using thermal modelling software in AutoDesk Inventor. The modelled demonstrated that the parts of the heat-sink furthest from the water would increase in temperate by 23ºC. This is well within the 75ºC nominal temperature limit of the most sensitive components in the transmitter circuitry.

In Figure 29 we plot the internal temperature of the EODTx50M transmitter as a function of time during a wet-test at Ostrich Bay in June 2021. Each transmitter was outputting approximately 50 A. Estimated water temperature at the time was around 9.5ºC. The temperature on each line starts off slightly higher as the tow-fish was brought to the surface at the end of each line. The system never gets over 32 ºC.

The EODTx120M will need to dissipate approximately 500 W through each of three transmitters (3000 W at 50% duty cycle with each transmitter operational for 1/3 of each second). We will model the expected heat dissipation using AutoDesk Inventor with the existing heat sink. As only three transmitters and not five are required, the heat sink size can be increased while keeping the enclosure size the same. In addition, if we need to further improve heat dissipation we can modify the heat sink to replace the air-cavity with a water tunnel that runs through the middle of the transmitter enclosure. This would provide additional cooling and reduce the temperature differential within the enclosure.

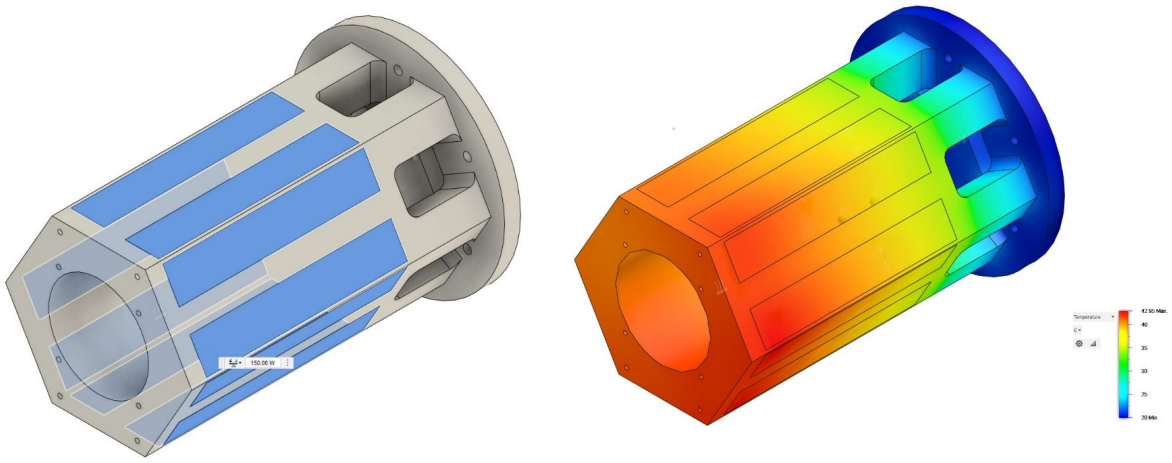

Figure 28. CAD model of the heat-sink in the EODTx50M transmitter. The blue panels show the locations of the heat-dissipating parts of each transmitter board. The temperature model on the right shows the steady state temperature assuming a water temperature of 20 ºC and 150 W power dissipation on each blue face. The heat-map range is 20 ºC (blue) to 43 ºC (red).

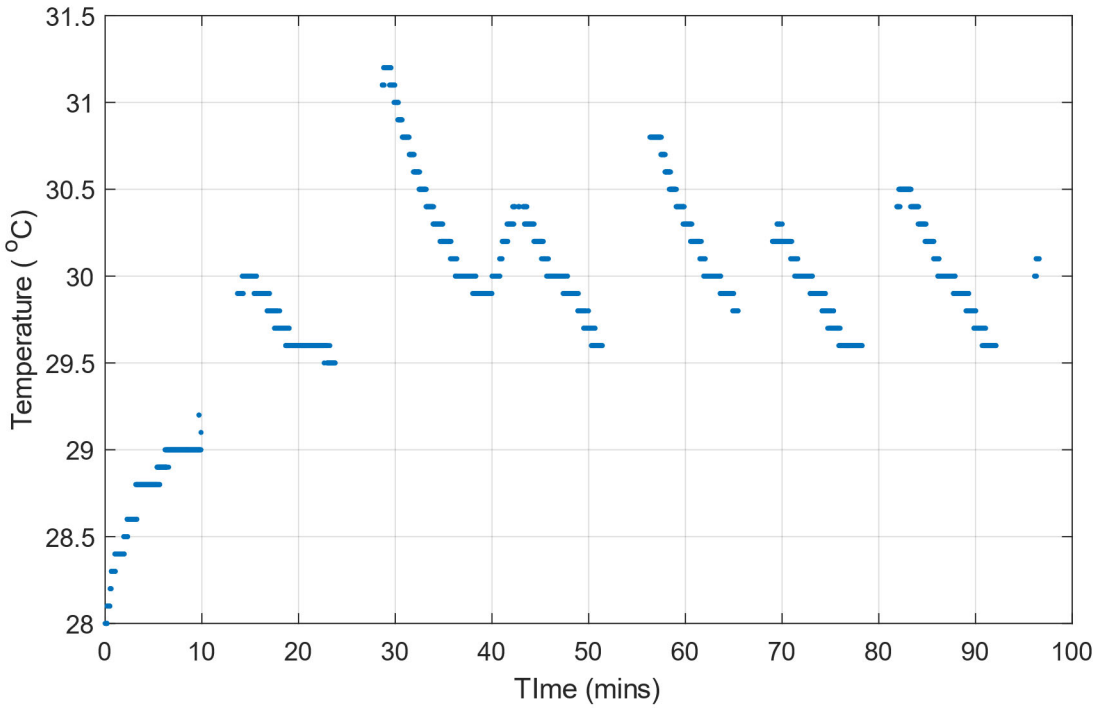

Figure 29. EODTx50M internal temperature as a function of time for a wet-test at Ostrich Bay in June 2021 with the transmitters outputting 50 A each.

Appendix B: Noise analysis of the TEMA system

The material in this appendix has been partly derived from the shakedown test report on the ESTCP MR19-5073 project.

As an indication of the noise expected to be encountered by the MTA system, we analyzed data from an UltraTEMA shakedown survey collected at Ostrich Bay, WA in June 2021. A number of transects were collected with the system flying at a nominal 1 m off the sea-bottom. For target picking and visualization of the UltraTEM data, a number of different transmitter/receiver combinations are interpolated onto a grid with regular 10 cm spacing (image formation). An image formed from a combination of Z-component data from receivers inside each transmitter is an effective product to use for target selection. This combination is known as "Inclusive Z" and is formed by using data from receivers 1 to 4 when transmitter 1 fires, receivers 5 to 8 when transmitter 2 fires and receivers 9 to 12 when transmitter 3 fires.

To provide an estimate of noise we selected five locations free of obvious anomalies and computed the Root Mean Square (RMS) of the detrend filtered early time-channel data within a 5 m long section of the Northward collected survey. The average of the RMS noise for each transmitter and receiver combination was then calculated (Table 2). The derived noise estimates vary from 0.025 uV/A to 0.3 uV/A. Assuming that targets are picked using what we term the Z-Inclusive components (grey highlighted cells in Table 2) we compute an average noise level of 0.171 uV/A in the early time composite channel. Assuming a detection limit of five times the noise results in a minimum target picking threshold of 0.86 uV/A.

We used the UXOLab Detection Modeller tool to estimate the standoff distance for an M314A3 105 mm projectile in the DoD TOI Library (Figure 30). At 2.2 m standoff depth the worst-case orientation of the 105 mm projectile model has an amplitude under the 0.86 uV/A threshold whereas the amplitudes for the vertical component orientations exceed that threshold across the entire swath width. Detection modeler in this case provides a somewhat pessimistic view of the detection depth, because the worst-case orientations are comparatively rare and the analysis doesn't account for the multiple transmitter-receiver combinations that are used for detection. At large standoffs multiple receivers will have comparable amplitude signals and there is an increased likelihood that at least one of them will exceed the detection threshold.

In any case, with the TEMA platform and the existing EODTx50M transmitter design, reliable detection to a 3 m standoff range would be difficult. Detection modeler amplitudes are always calculated assuming the transmitter has a single turn and 1 A of current. For multiple turn transmitters and large currents, the receiver data are normalized by the A·turns in the loop (so units are in uV/A) and the Detection Modeler thresholds are applicable (since the transmitter has effectively been transformed into a single turn with 1 A of current). The noise experienced by the receiver in uV is also divided by A·turns when converting to units of uV/A. This means that if the absolute value of the noise doesn't change when increasing the transmitter current that the noise-floor decreases as one over the A·turns in the transmitter. The signal to noise ratio (SNR), in turn, increases in direct proportion to the A·turns in the transmitter. For example, increasing the number of A·turns by a factor of two decreases the size of the noise in uV/A by a factor of two and increases the SNR by a factor of two.

In Figure 31 we compare the noise floor for a one-minute static measurement for a 12-turn loop with 100 Amps when the transmitter is on to when it was off. Beyond approximately 200 us, the noise floor is equivalent between the two cases for the Z-component which is maximally coupled with the transmitter field direction. Thus, our assumption that the noise is independent of the transmitter current is valid for the time-range of interest for marine EMI sensing.

To summarize: Detection Modeler amplitudes are calculated in units of uV/A. As the number of Amp-turns increases, the SNR at a given amplitude threshold increases in direct proportion to the Amp-turns. With a comparable sized transmitter loop, the noise floor would have to decrease by a factor of about 3 to 4 for detection to be feasible (Figure 32).

Table 2. Average RMS noise of the early time-composite channel across five background locations. The grey highlighted cells show the Inclusive Z-component data used for initial target selection. The bottom row shows the average for each transmitter with the average across transmitters shown as the last entry.

	Tx1	Tx2	Tx3	Tx4
Rx1	0.163	0.141	0.166	0.056
Rx2	0.087	0.178	0.198	0.322
Rx3	0.146	0.170	0.137	0.063
Rx4	0.058	0.222	0.046	0.025
Rx5	0.246	0.126	0.290	0.296
Rx6	0.279	0.263	0.071	0.085
Rx7	0.169	0.175	0.283	0.176
Rx8	0.175	0.300	0.219	0.300
Rx9	0.132	0.286	0.229	0.036
Rx10	0.096	0.218	0.083	0.117
Rx11	0.128	0.142	0.265	0.170
Rx12	0.147	0.096	0.153	0.103
Inclusive-Z	0.113	0.216	0.183	0.171

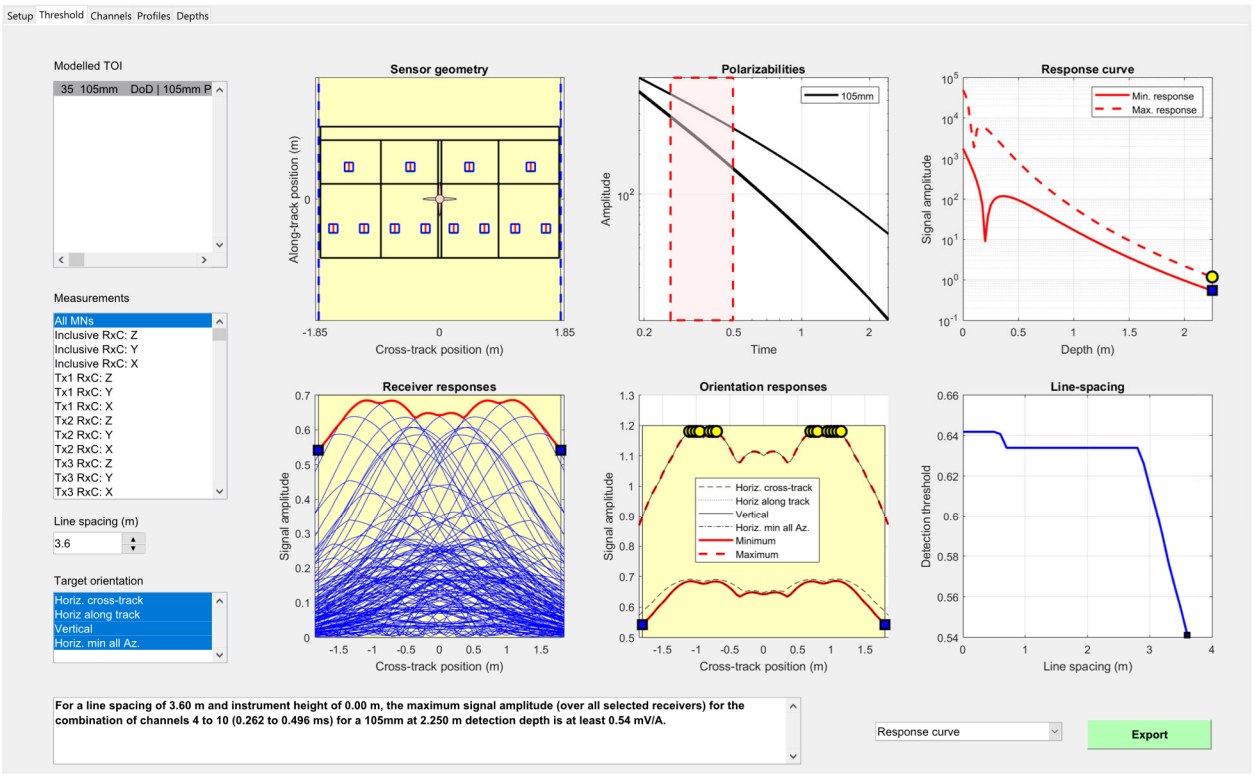

Figure 30. TEMA 4 Detection Modeller analysis of a 105 mm projectile at a stand-off distance of 2.2 m.

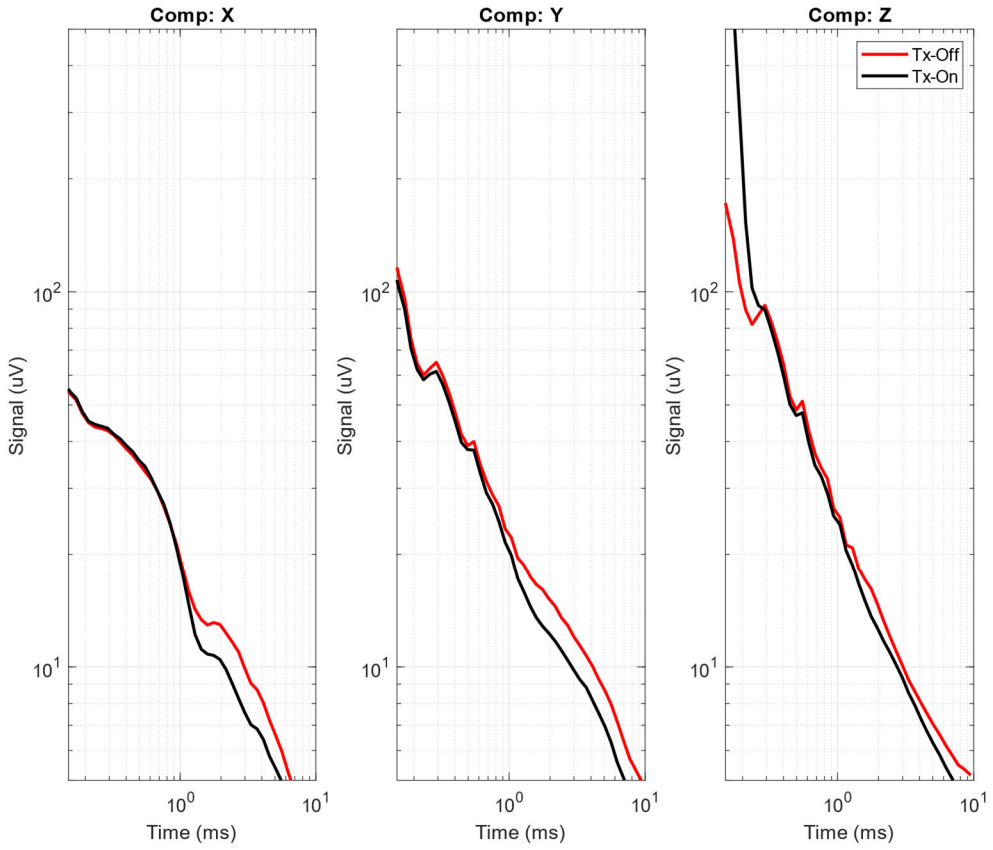

Figure 31. Noise comparison obtained with the 12 turn loop operating at 100 Amps provides an example of the noise (in uV) when the transmitter is operating compared to when it is off. The noise beyond about 200 us is comparable between Tx on and Tx off and it's only at the early times where the noise is larger for Tx on for the Z-component (which is in-line with the transmitter field).

For comparison, we have run the same models using the MTA configuration, included in Figure 33 and Figure 34. Assuming the same number of Ampere-turns as the UltraTEMA system, the larger size of the main transmitter loop in the MTA results in a slower fall-off in the primary field and an increased threshold at both 2.2 and 3 m standoff. With the same detection threshold as the UltraTEMA system (0.86 uV/A), reliable detection of a 105 mm at a standoff distance of 3 m would not be possible. An increase in the transmitter current of a factor of 2.5 to 4 would be required to achieve the required stand-off objective.

We also performed a more detailed analysis of the noise for each individual time-channel (Figure 35 and Table 3. For this analysis we calculated the noise floor for each of the five background regions for each transmitter/receiver combination (grey lines). We also calculated the average noise floor across all transmitter/receiver combinations (solid black line in each plot).

The noise floor analysis for the UltraTEMA4 shakedown survey collected at Ostrich Bay in June 2021 is plotted along with the levels seen for the MTA on the York River and our proof-of-

concept measurements from Australia in October and November, 2021(taken from Figure 25). The terrestrial noise levels we were seeing in Australia in 2021 correspond with the levels we observed in the York River, VA in 2019. The Ostrich Bay, WA UltraTEMA4 noise levels were comparable. However, experience tells us that noise floors are going to be site- and time-dependent and that being overly aggressive in designing against a low noise floor could have significant impacts in classification performance.

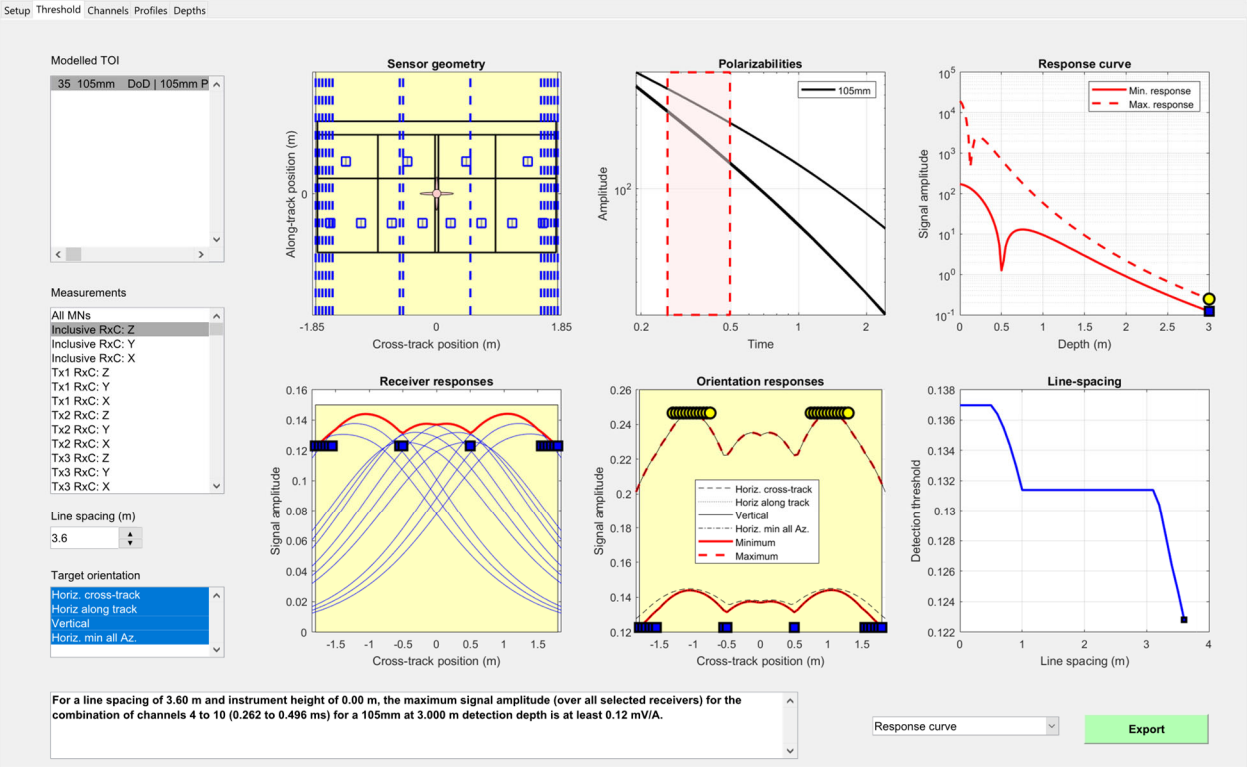

Figure 32. TEMA 4 Detection Modeller analysis of 105 mm projectile at a stand-off distance of 3.0 m.

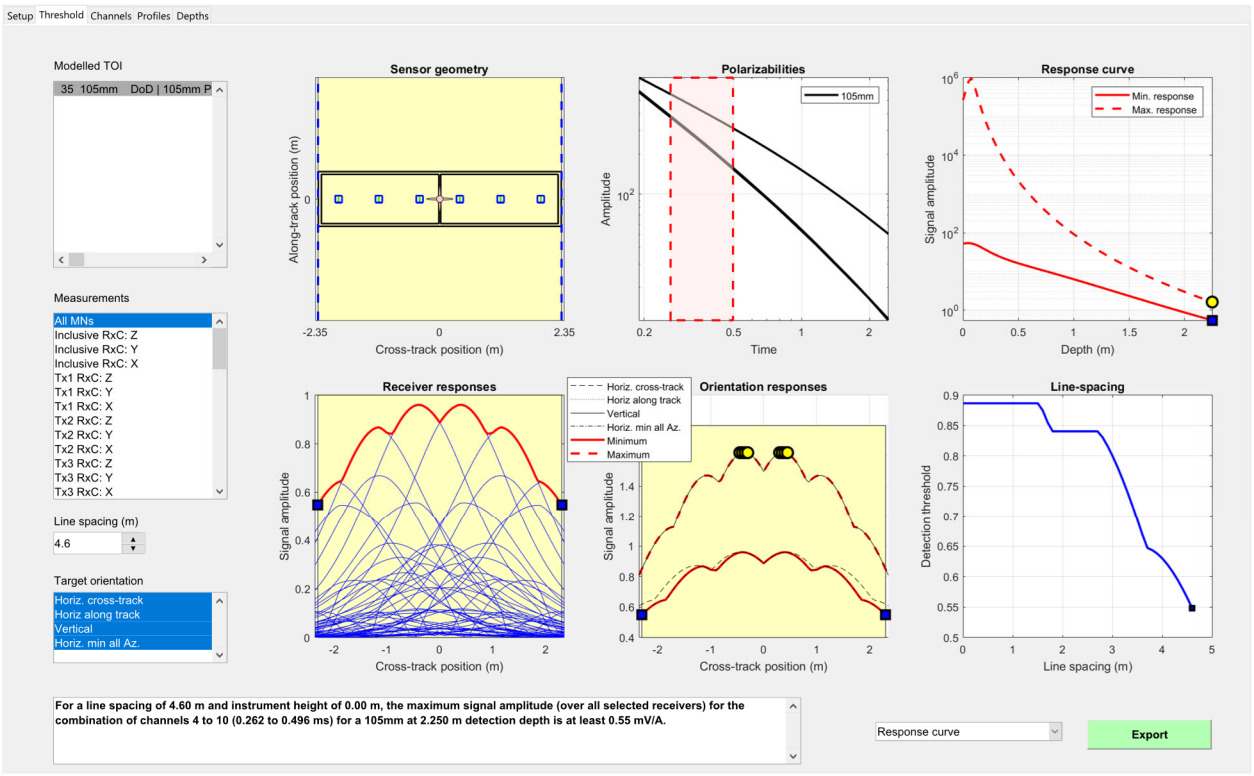

Figure 33. MTA Detection Modeller analysis of a 105 mm projectile at a stand-off distance of 2.2 m.

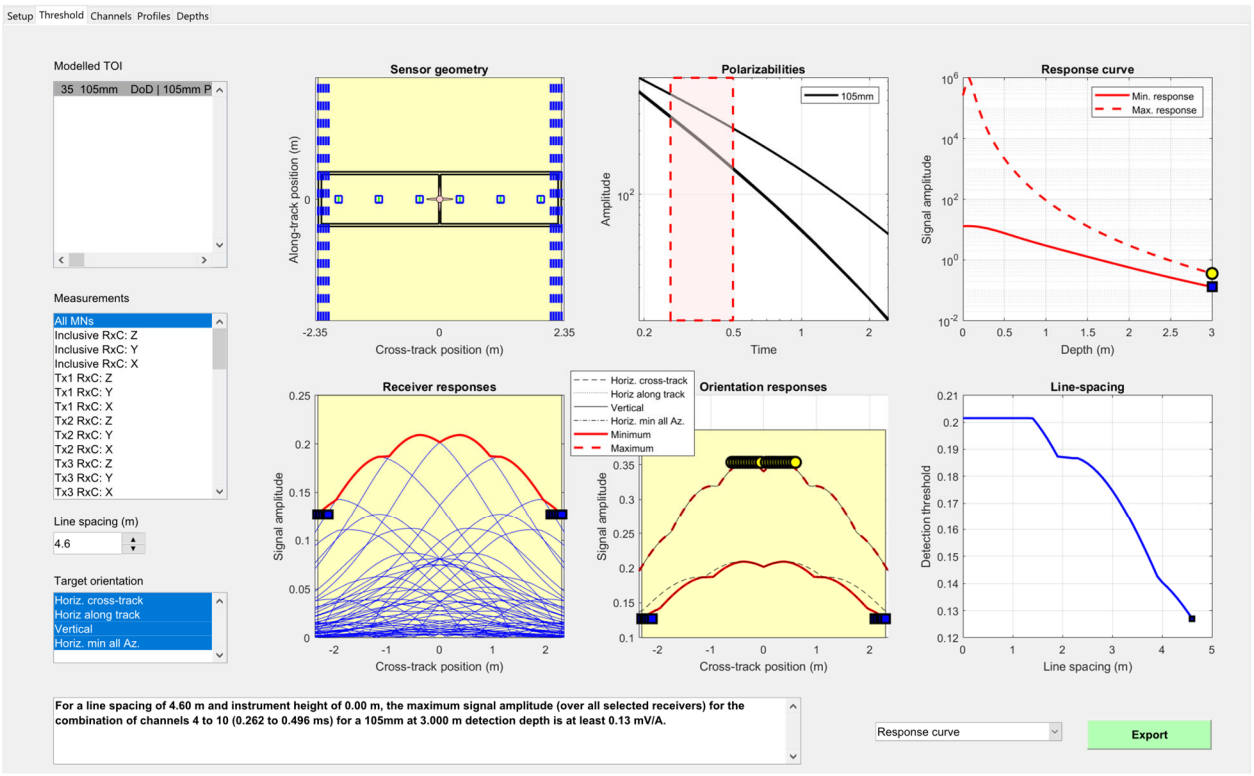

Figure 34. MTA 4 Detection Modeller analysis of 105 mm projectile at a stand-off distance of 3.0 m.

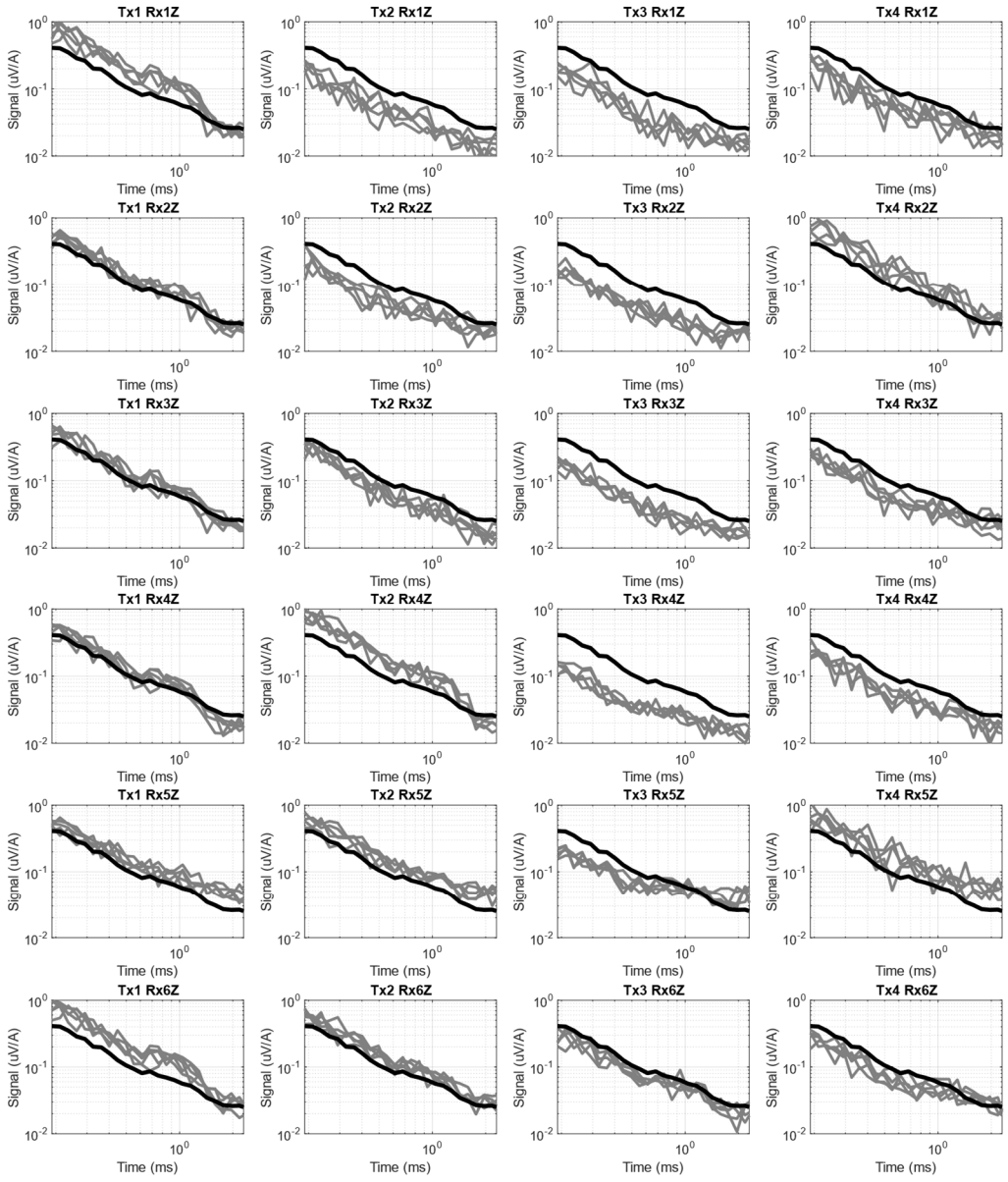

Figure 35**. RMS noise for all transmitter receiver combinations in the TEMA system (transmitters are left to right and receivers are top to bottom). Grey lines are the RMS noise estimates for the 5 different locations and the solid black line is the average noise across all samples. Only the receivers from the left hand side of the TEMA are shown.**

Table 3. Average RMS noise for the TEMA system operating in Ostrich Bay.

Time-Channel	RMS noise (uV/A)
0.19	0.410
0.211	0.403
0.235	0.351
0.262	0.287
0.292	0.263
0.325	0.201
0.361	0.197
0.401	0.161
0.446	0.127
0.496	0.107
0.551	0.094
0.613	0.081
0.681	0.086
0.758	0.074
0.842	0.069
0.936	0.063
1.04	0.056
1.156	0.052
1.286	0.044
1.429	0.035
1.588	0.031
1.764	0.027
1.961	0.026
2.178	0.026
2.42	0.024

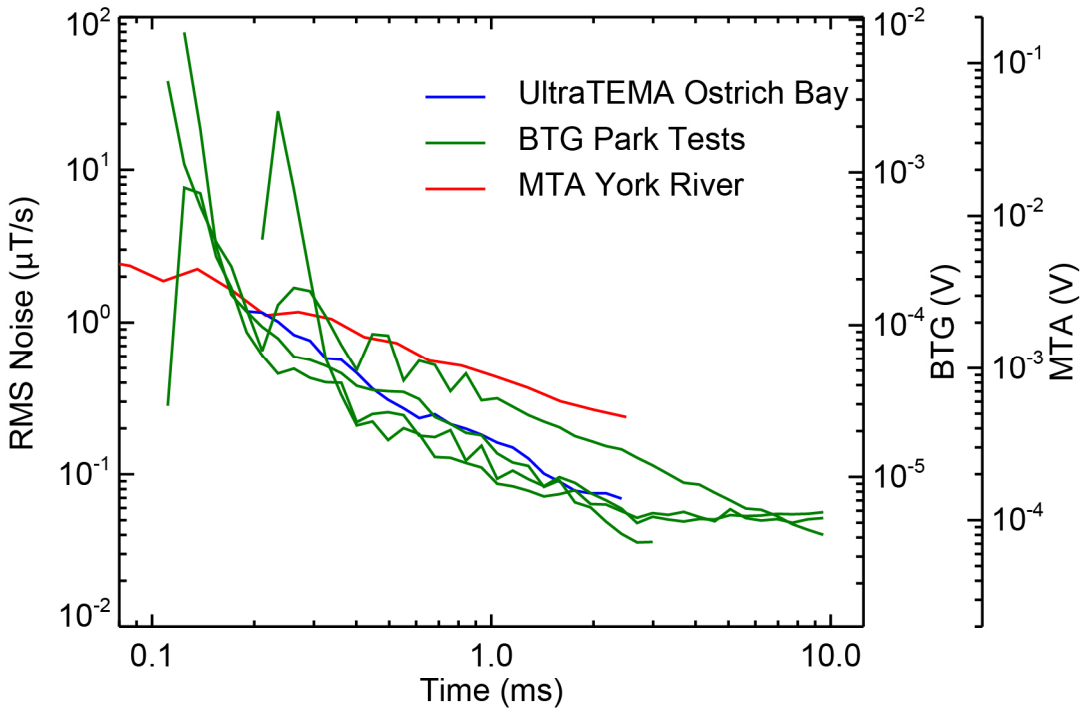

Figure 36. Noise comparison between BTG and MTA data collections. The BTG Park data was collected in Fall 2021 in a terrestrial setting in Australia. The MTA data was collected in the York River, VA in Winter 2019. The UltraTEMA data was collected in Ostrich Bay, WA in June 2021.